1 **Protein Phosphatase 1 in association with Bud14 inhibits mitotic exit in *Saccharomyces***
2 ***cerevisiae***

3 **Dilara Kocakaplan[1, ‡], Hüseyin Karabürk[1, ‡], Cansu Dilege[1], Idil Kirdok[1], Şeyma Nur**
4 **Bektaş[1], Ayse Koca Caydasi[1, *]**

5 [1]Department of Molecular Biology and Genetics, Koç University, Istanbul, Turkey

6 [‡]These authors contributed equally to this work

7 *Correspondence to: aykoca@ku.edu.tr

8

Abstract

Mitotic exit in budding yeast is dependent on correct orientation of the mitotic spindle along the cell polarity axis. When accurate positioning of the spindle fails, a surveillance mechanism named the Spindle Position Checkpoint (SPOC) prevents cells from exiting mitosis. Mutants with a defective SPOC become multinucleated and lose their genomic integrity. Yet, a comprehensive understanding of the SPOC mechanism is missing. In this study, we identified the type 1 protein phosphatase, Glc7, in association with its regulatory protein Bud14 as a novel checkpoint component. We further showed that Glc7-Bud14 promotes dephosphorylation of the SPOC effector protein Bfa1. Our results suggest a model in which two mechanisms act in parallel for a robust checkpoint response: first, the SPOC kinase Kin4 isolates Bfa1 away from the inhibitory kinase Cdc5 and second, Glc7-Bud14 dephosphorylates Bfa1 to fully activate the checkpoint effector.

22 **Introduction**

23 Budding yeast undergoes asymmetric cell division in every cell cycle and is an intrinsically
24 polarized cell. In every cell cycle, a new cell buds on the mother cell and pinches of from this
25 location at the end of the cell division, giving rise to a young daughter cell and an old mother
26 cell. In order for the daughter cell to receive one copy of the duplicated genetic material,
27 budding yeast has to segregate its chromosomes along its mother-to-bud polarity axis, which
28 requires positioning of the mitotic spindle apparatus along this direction. The correct
29 orientation of the mitotic spindle is achieved by two redundant pathways, namely the "early"
30 and "late" pathways, which are dependent on the Adenomatous Polyposis Coli (APC) homolog
31 Kar9 and the microtubule motor protein Dyn1 respectively (Adames & Cooper, 2000; Beach
32 *et al*, 2000; Li *et al*, 1993; Siller & Doe, 2009).

33 Correct orientation of the mitotic spindle is monitored by a mitotic checkpoint named the
34 Spindle Position Checkpoint (SPOC) in budding yeast. SPOC prevents cell cycle progression
35 of cells that fail to orient their spindle in the mother-to-bud direction, and hence provides time
36 for cells to correct their spindle orientation before mitotic exit (Adames *et al*, 2001; Bardin *et*
37 *al*, 2000; Bloecher *et al*, 2000; Pereira *et al*, 2000; Yeh *et al*, 1995). Yeast cells with defects in
38 the spindle positioning pathways or cells with impaired microtubule function rely on the SPOC
39 to maintain their ploidy. Absence of SPOC causes multinucleation, enucleation and aneuploidy
40 in budding yeast. A SPOC like checkpoint also exists in Drosophila and may be present in
41 higher eukaryotes (Cheng *et al*, 2008; O'Connell & Wang, 2000; Pereira & Yamashita, 2011).

42 In response to spindle mispositioning, SPOC inhibits cell cycle progression by inhibiting the
43 Mitotic Exit Network (MEN) (Baro *et al*, 2017; Caydasi *et al*, 2010a; Caydasi & Pereira, 2012;
44 Weiss, 2012). MEN is a GTPase driven signaling pathway that is essential for mitotic exit in
45 budding yeast (Jaspersen *et al*, 1998; Shou *et al*, 1999). A single conserved phosphatase, named

46 Cdc14 triggers mitotic exit in budding yeast through inactivation of the mitotic Cyclin
47 Dependent Kinase (CDK) and dephosphorylation of CDK targets (Manzano-Lopez & Monje-
48 Casas, 2020). At the anaphase onset, a transient wave of Cdc14 activation is triggered by the
49 cdcFourteen Early Anaphase Release (FEAR) network; whereas later in anaphase the MEN
50 promotes fully activation of Cdc14 (Jaspersen *et al.*, 1998; Lee *et al*, 2001a; Rock & Amon,
51 2009; Shou *et al.*, 1999). A Ras-like small GTPase named Tem1 is the main switch located
52 near the top of the MEN (Lee *et al.*, 2001a; Morishita *et al*, 1995; Scarfone & Piatti, 2015;
53 Shirayama *et al*, 1994b). When bound to GTP, Tem1 initiates the MEN signaling by recruiting
54 the Cdc15 kinase to the spindle pole bodies (centrosome equivalent in yeast, SPB) which
55 therein activates Dbf2 kinase in association with its regulatory subunit Mob1 (Asakawa *et al*,
56 2001; Cenamor *et al*, 1999; Visintin & Amon, 2001).

57 SPOC inhibits the MEN through inactivation of Tem1 by a bipartite GTPase Activating
58 Complex (GAP) composed of Bfa1 and Bub2 proteins (Geymonat *et al*, 2002). Activity of the
59 Bfa1-Bub2 GAP complex is tightly regulated at the level of Bfa1 phosphorylation. In cells with
60 a correctly positioned anaphase spindle, the polo like kinase Cdc5 phosphorylates Bfa1 to
61 prevent Bfa1-Bub2 GAP activity towards Tem1 (Hu *et al*, 2001). CDK also phosphorylates
62 Bfa1 in an activating manner until anaphase when this phosphorylation is removed in a FEAR
63 related manner (Caydasi *et al*, 2017). In the presence of spindle misalignment, however, Kin4
64 kinase phosphorylates Bfa1 (Maekawa *et al*, 2007). This phosphorylation prevents inhibitory
65 phosphorylation of Bfa1 by Cdc5 kinase (Pereira & Schiebel, 2005). Consequently, Bfa1-Bub2
66 GAP complex activity is promoted, Tem1 activity is prevented, and exit from mitosis is
67 inhibited.

68 SPBs, serving as a scaffold, play a key role in mitotic exit and its timely regulation by the
69 spindle position (Campbell *et al*, 2020; Gruneberg *et al*, 2000; Pereira & Schiebel, 2001;

70 Valerio-Santiago & Monje-Casas, 2011). When the spindle is properly oriented, Bfa1-Bub2
71 and Tem1 reside in a preferential, asymmetrical manner at the SPB that moves to the daughter
72 cell (dSPB) (Molk *et al*, 2004; Pereira *et al.*, 2000). On contrary, Kin4 localizes exclusively to
73 the SPB that stays in the mother cell (mSPB) during an unperturbed anaphase (D'Aquino *et al*,
74 2005; Pereira & Schiebel, 2005). Spindle misalignment alters SPB localization of SPOC
75 components. Upon mispositioning of the mitotic spindle, Kin4 localizes to both SPBs (Gislene
76 Pereira & Schiebel, 2005). Phosphorylation of Bfa1 by Kin4 promotes binding of the 14-3-3
77 family protein Bmh1 to Bfa1 which causes dissociation of Bfa1-Bub2 from SPBs (Caydasi *et*
78 *al*, 2012; Caydasi *et al*, 2014; Caydasi & Pereira, 2009; Monje-Casas & Amon, 2009). Hence,
79 upon spindle mispositioning, the amount of Bfa1-Bub2 at both SPBs decreases, while their
80 cytoplasmic levels increase. The release of Bfa1-Bub2 from SPBs is thought to keep Bfa1-
81 Bub2 away from the inhibitory kinase Cdc5 and thus prevent inactivation of Bfa1-Bub2 by
82 Cdc5. However, what dephosphorylates the Cdc5 phosphorylated Bfa1 remains elusive.

83 Here, we identified Bud14 as a novel SPOC protein. Deletion of *BUD14* rescued cold
84 sensitivity of *lte1*Δ cells, lethality of mitotic exit deficient *lte1*Δ *spo12*Δ cells, and growth
85 defects of MEN temperature sensitive mutants *cdc15-1*, *dbf2-2*, *mob1-67*. Our data showed
86 that *bud14*Δ cells accumulated multinucleated phenotypes when spindle positioning was
87 impaired in cells via deletion of *KAR9* or *DYN1*. Fluorescence time-lapse microscopy revealed
88 that *bud14*Δ cells failed to delay mitotic exit in response to spindle mispositioning. We
89 observed an additive decrease in anaphase duration of *kin4*Δ *bud14*Δ cells with misaligned
90 spindles compared to the cells bearing single gene deletions of *KIN4* or *BUD14* suggesting that
91 Kin4 and Bud14 work in parallel in SPOC. We further found that the mitotic exit inhibitory
92 function Bud14 required its association with the type 1 protein phosphatase, Glc7. A
93 temperature sensitive version of Glc7 (*glc7-12*) and a version of Bud14 that cannot interact
94 with Glc7 (*bud14-F379A*) caused SPOC deficiency and rescued growth of mitotic exit mutants.

95 Yeast two hybrid data indicated an interaction between Bfa1 and Bud14 that required the
96 presence of Bub2, which suggests that Bud14 may recognize Bfa1-Bub2. Intriguingly, *bud14*Δ
97 and *bud14-F379A* cells had more Bfa1-Bub2 localized at the dSPBs, suggestive of a role for
98 Bud14-Glc7 in limiting SPB-bound levels of Bfa1-Bub2. Similarly to the wild type cells, upon
99 spindle mispositioning, levels of Bfa1 at the dSPB was able to decrease in *bud14*Δ cells, unlike
100 *kin4*Δ cells, which also supported separate functions of Bud14 and Kin4 in SPOC. We further
101 observed that *lte1*Δ cells lacking Bud14 accumulated hyperphosphorylated Bfa1 forms during
102 anaphase. Furthermore, overexpression of *BUD14* but not *bud14-F309A* caused a reduction in
103 this hyperphosphorylated forms of Bfa1. Finally, through in vitro phosphatase assays we
104 showed that Glc7-Bud14 promoted dephosphorylation of hyperphosphorylated Bfa1. Our data
105 altogether indicates that Glc7-Bud14 is a novel mitotic exit inhibitor in budding yeast that
106 works upon spindle mispositioning. We propose a checkpoint model in which two independent
107 mechanisms activate the checkpoint effector: first, the SPOC kinase Kin4 prevents further
108 Cdc5 phosphorylation of Bfa1 by rapidly removing Bfa1 away from the Cdc5 kinase and
109 second, Glc7-Bud14 dephosphorylates Bfa1 to activate the Bfa1-Bub2 GAP complex. Both
110 mechanisms are crucial for rapid activation of the checkpoint effector Bfa1-Bub2 upon
111 mispositioning of the anaphase spindle.

112

113 **Results**

114 **Bud14 is a Novel Mitotic Exit Inhibitor**

115 Lte1 is a mitotic exit activator that becomes essential for mitotic exit at cold temperatures (<16
116 ºC) (Shirayama *et al*, 1994a). Although the exact function of Lte1 in mitotic exit is not fully
117 understood, one of the ways that Lte1 promotes mitotic exit is by preventing binding of the
118 SPOC kinase Kin4 to the SPB that has migrated into the bud and by inhibiting its activity
119 therein (Bertazzi *et al*, 2011; Falk *et al*, 2011). At physiological temperatures (i.e. 30 ºC) *lte1*Δ
120 cells rely on the presence of the FEAR network to exit mitosis. Deletion of FEAR network
121 components such as *SPO12* or *SLK19* in *lte1*Δ cells causes lethality due to failure of mitotic
122 exit (Stegmeier *et al*, 2002). Lethality of the *lte1Δ spo12Δ* double mutants can be rescued by
123 deletion of the known mitotic exit inhibitors *BFA1*, *BUB2* and *KIN4* (D'Aquino *et al.*, 2005;
124 Stegmeier *et al.*, 2002). In order to identify novel mitotic exit inhibitors, we designed a genetic
125 screen that looked for single gene deletions rescuing *lte1Δ spo12Δ* lethality. In addition to the
126 known mitotic exit inhibitors *BFA1*, *BUB2* and *KIN4*, we identified *BUD14* as a novel gene
127 that contributes to the mitotic arrest of *lte1Δ spo12Δ* cells (data not shown). Deletion of *BUD14*
128 rescued lethality of *lte1Δ spo12Δ* cells (Figure 1A). Deletion of *BUD14* also rescued the cold
129 sensitivity of *lte1Δ* cells (Figure 1B). This data indicates that Bud14 is a novel inhibitor of
130 mitotic exit.

131 We next asked whether deletion of *BUD14* rescues growth lethality of mitotic exit network
132 (MEN) mutants. For this, we deleted *BUD14* in several MEN temperature sensitive (ts) mutants
133 (Jaspersen *et al.*, 1998) and compared their growth at different temperatures. To allow for better
134 comparison, we also deleted *BFA1*, a known mitotic exit inhibitor, in the same MEN-ts mutants
135 (Caydasi *et al.*, 2017; Hu *et al.*, 2001; Pereira *et al.*, 2000; Scarfone *et al*, 2015; Wang *et al*,
136 2000). In line with its mitotic exit inhibitory role, deletion of *BFA1* rescued the lethality of

137 *mob1-67*, *dbf2-2, cdc15-1 and cdc5-10* ts mutants at 33 °C, 37 °C, 35 °C and 37 °C respectively
138 (Figure 1C). Deletion of *BUD14* also promoted the growth of *mob1-67*, *dbf2-2*, and *cdc15-1*
139 mutants at 33 °C, 35 °C and 35 °C respectively (Figure 1C). In all cases, growth rescue by
140 *BUD14* deletion was milder than that of *BFA1* deletion. Furthermore, *BUD14* deletion did not
141 rescue the growth of the *cdc5-10* while *BFA1* deletion did (Figure 1C), suggesting that the
142 mitotic exit inhibitory function of Bud14 does not contribute to *cdc5-10* lethality. Deletion of
143 neither *BFA1* nor *BUD14* rescued the growth of the *cdc14-2* mutant (Figure 1C). Cdc14 is the
144 essential phosphatase that is activated at the very downstream of the MEN pathway. The fact
145 that *bud14*Δ and *bfa1*Δ does not rescue *cdc14-2* supports their function upstream of the MEN
146 pathway.

147 ***BUD14* is essential for SPOC functionality**

148 The known mitotic exit inhibitors Bfa1, Bub2 and Kin4 are key components of the Spindle
149 Position Checkpoint (SPOC), which is a surveillance mechanism that inhibits the MEN when
150 anaphase spindle fails to orient in the mother-to-daughter direction. We thus asked whether the
151 novel mitotic exit inhibitor Bud14 has a role in SPOC. To address this, we first employed a
152 population-based approach. Cells with a functional SPOC, arrest in anaphase with
153 mispositioned nuclei upon spindle mispositioning, whereas SPOC deficient cells such as *bfa1*Δ
154 or *kin4*Δ continue cell cycle progression resulting in formation of multinucleated and
155 enucleated cells. We assayed SPOC deficiency in cell populations as a measure of frequency
156 of multinucleation, relative to that of the spindle mispositioning (SPOC deficiency index).
157 Kar9- and Dynein-dependent spindle positioning pathways act redundantly to align the spindle
158 along mother-to-daughter polarity axis in budding yeast (Eshel *et al*, 1993; Li *et al.*, 1993;
159 Miller & Rose, 1998). To induce spindle mispositioning, we first made use of *kar9*Δ cells. As
160 expected, deletion of known SPOC components *KIN4* or *BFA1* in the *kar9*Δ background

161 yielded a remarkably high degree of SPOC deficiency index (Figure 2A). Notably, deletion of
162 *BUD14* in the *kar9*Δ background also caused a significantly high SPOC deficiency index
163 (Figure 2A). Similar results were obtained using a *dyn1*Δ background (Figure 2B). These data
164 suggests that *bud14*Δ cells are defective in SPOC.

165 We then employed a single cell analysis approach to assay SPOC functionality. For this, we
166 analyzed the timing of mitotic exit in *bud14*Δ cells during spindle misalignment and normal
167 alignment in a *GFP-TUB1 kar9*Δ cell background. *GFP-TUB1* served as a spindle marker.
168 *kar9*Δ population contains cells with misaligned spindles as well as cells with normally aligned
169 spindles, and thus allows analysis of anaphase duration in both cases. Cells were imaged
170 through fluorescence time-lapse microscopy for 90 minutes with 1 min time-resolution at 30
171 ºC. Anaphase duration was calculated as the time elapsed between the start of fast spindle
172 elongation and the spindle breakage, which are indications of anaphase onset and mitotic exit
173 respectively. In cells with a normally positioned spindle, mean anaphase duration of all
174 analyzed cell types were similar - ranging from 18 to 19 minutes with a standard deviation of
175 2 minutes (Figure 2C, Source data Figure 2C). The majority of *kar9*Δ cells with a misaligned
176 spindle stayed arrested with an intact spindle during the time-lapse movie (Figure 2C, *kar9*Δ
177 red triangles), whereas *kin4*Δ *kar9*Δ cells with misaligned spindles broke their anaphase spindle
178 in average 27±7 minutes (mean± standard deviation) after the onset of anaphase (Figure 2C,
179 *kar9*Δ *kin4*Δ black squares). *bud14*Δ *kar9*Δ cells with misaligned spindles also broke their
180 spindle and with a mean anaphase duration of 23 ± 4 minutes (mean± standard deviation)
181 (Figure 2C, *kar9*Δ *bud14*Δ, black squares). These data altogether suggest that Bud14 is needed
182 as a part of the SPOC mechanism to delay mitotic exit upon spindle mispositioning.

183 **Function of Bud14 in SPOC is parallel to Kin4**

184 Bfa1-Bub2 is the most downstream component of SPOC and Kin4 is the key SPOC kinase that
185 resides upstream of Bfa1 to promote Bfa1-Bub2 GAP activity upon spindle misalignment. We
186 next asked whether Bud14 work parallel to Kin4 in SPOC. We reasoned that if Bud14 and
187 Kin4 work in parallel, concomitant loss of Bud14 and Kin4 would cause a greater SPOC
188 deficiency index than individual loss of Bud14 or Kin4. SPOC deficiency index of *kin4*Δ
189 *bud14*Δ *kar9*Δ was significantly higher than that of *kin4*Δ *kar9*Δ or *bud14*Δ *kar9*Δ (Figure 2A).
190 Likewise, SPOC deficiency phenotype was more prominent in *kin4*Δ *bud14*Δ *dyn1*Δ cells than
191 in *kin4*Δ *dyn1*Δ or *bud14*Δ *dyn1*Δ cells (Figure 2B). Thus, *KIN4* and *BUD14* deletion showed
192 an additive effect with respect to SPOC deficiency. Of note, deletion of *BUD14* in *bfa1*Δ *kar9*Δ
193 cells did not cause any increase in SPOC deficiency index compared to *bfa1*Δ *kar9*Δ cells
194 (Figure 2A). These data are suggestive of a role for Bud14 parallel to Kin4 and upstream of
195 Bfa1 and in SPOC.

196 Additive effect of *KIN4* and *BUD14* deletion was also evident in anaphase duration
197 comparisons. Even though *BUD14* deletion caused mitotic exit of cells with misaligned
198 spindles, duration of anaphase in *bud14*Δ *kar9*Δ cells was significantly longer during spindle
199 misalignment than during spindle normal alignment (Figure 2C, *bud14*Δ, squares vs circles).
200 In addition, one out of 18 cells was able to hold the SPOC arrest longer than an hour. Similar
201 phenomenon was also observed in *kar9*Δ *kin4*Δ cells (Figure 2C, *kin4*Δ, squares vs circles) and
202 was also reported before (Caydasi *et al.*, 2017; Falk *et al*, 2016b). This indicates that in the
203 absence of Bud14 or Kin4, cells are still able to delay mitotic exit in response to spindle
204 positioning defects, albeit for short time. On contrary, when both *KIN4* and *BUD14* were
205 deleted, cells exited mitosis with the same timing regardless of the spindle position (Figure 2C,
206 *kar9*Δ *bud14*Δ *kin4*Δ black squares vs circles). Thus, concomitant deletion of *KIN4* and *BUD14*

207 results in a more severe loss of SPOC functionality than single deletion of either *KIN4* or
208 *BUD14*. This data is in line with our conclusion that Kin4 and Bud14 act in parallel to promote
209 SPOC arrest.

210 To rule out the possibility that Bud14 may also be acting upon Kin4, we next analyzed the
211 effect of Bud14 on Kin4 functionality. For this, we first analyzed cells overexpressing Kin4.
212 Kin4 overexpression blocks exit from mitosis through constitutive Bfa1-Bub2 activation and
213 thus results in lethality (D'Aquino *et al.*, 2005). This lethality can be rescued by deletion of
214 *BFA1* or *BUB2,* which are the most downstream SPOC components, and by deletion of *RTS1*
215 or *ELM1*, which are Kin4 regulators, and by deletion of *BMH1*, which works downstream of
216 *KIN4* (Caydasi *et al*, 2010b; Caydasi *et al.*, 2014). Unlike aforementioned gene deletions,
217 deletion of *BUD14* did not rescue the lethality of Kin4 overexpression (Figure 2 – Figure
218 Supplement 1A). Thus, overproduced Kin4 is still able to activate Bfa1 constitutively in the
219 absence Bud14. Next, we analyzed the effect of Bud14 on Kin4 localization. Kin4 localized to
220 SPBs in response to microtubule depolymerization independently of the presence of Bud14
221 (Figure 2 – Figure Supplement 1B). Likewise, Kin4 localized to SPBs during anaphase in *lte1*Δ
222 cells both in the presence and absence of Bud14 (Figure 2 – Figure Supplement 1C). Kin4
223 mobility on SDS-PAGE was not altered in cells lacking Bud14 either (Figure 2 – Figure
224 Supplement 1D). These data indicate that Bud14 does not work upstream of Kin4. As we will
225 describe later, analysis of Bfa1 localization during spindle misalignment also supported that
226 Kin4 regulation of Bfa1 takes place independently of Bud14 (Figure 6D, Figure 6- Supplement
227 3). Taken altogether, our data support a model where Bud14 acts in a pathway parallel to Kin4
228 in SPOC.

229 **Bud14 function in SPOC is independently of its role in actin regulation**

230 Bud14 regulates actin cable formation through its formin-regulatory motif (amino acids 135-
231 150) (Chesarone *et al*, 2009; Eskin *et al*, 2016). Bud14's function in controlling formin activity
232 also requires its interaction with KELCH domain proteins Kel1 and Kel2 (Gould *et al*, 2014).
233 We addressed the contribution of actin regulatory role of Bud14 to its mitotic exit inhibitory
234 function through two independent approaches. First, we made use of the *bud14-5A* mutant
235 whose formin-regulatory motif is disrupted by five alanine amino acid substitutions at Bud14
236 residues 135 and 137–140 (Eskin *et al.*, 2016). Ectopic expression of *bud14-5A* and *BUD14*
237 on a centromeric yeast plasmid (pRS416) under *BUD14* endogenous/native promoter rescued
238 the SPOC deficient phenotype of *bud14*Δ *kar9*Δ cells (Figure 3A) (Figure 3 – Figure
239 supplement 1A). Similarly ectopic expression of *bud14-5A* in *lte1*Δ *bud14*Δ cells
240 complemented *BUD14* deletion by restoring cold sensitivity of *lte1*Δ (Figure 3B). Thus, *bud14-*
241 *5A* mutant, which is deficient in formin binding is functional in terms of mitotic exit inhibition.
242 Of note, expression of *bud14-5A* caused a significantly greater extend of reduction in SPOC
243 deficiency index of *bud14*Δ *kar9*Δ cells than expression of *BUD14* (Figure 3A). Furthermore,
244 Bud14-5A interacted with Glc7 more readily in yeast two hybrid assays (Figure 3 – Figure
245 supplement 1B), which may indicate a link between Glc7-Bud14 interaction and SPOC
246 robustness.

247 Second, we made used of *kel1*Δ and *kel2*Δ cells. Kel1, Kel2 and Bud14 form a stable complex
248 that regulate the formin Bnr1 and any missing protein from this complex causes actin cable
249 defects to the same extend (Gould *et al.*, 2014). We reasoned that if Kel1-Kel2-Bud14 complex,
250 that is crucial for actin regulation, is also important for SPOC functionality, deletion of *KEL1*
251 or *KEL2* to disturb the complex would also cause SPOC deficiency similar to the *bud14*Δ cells.
252 However, this was not the case. Unlike *bud14*Δ *kar9*Δ cells, *kel1*Δ *kar9*Δ or *kel2*Δ *kar9*Δ cells

253 did not display SPOC deficiency (Figure 3C). These data altogether suggest that Bud14
254 function in SPOC is independent of its role in actin cable regulation.

255 Interestingly, deletion of *KEL1* also rescues cold sensitivity of *lte1*Δ similar to the deletion of
256 *BUD14* (Hofken & Schiebel, 2002; Seshan *et al*, 2002) (Figure 3D). Synthetic lethality of
257 *lte1*Δ *spo12*Δ on the other hand, can only be slightly rescued by the deletion of *KEL1*, whereas
258 deletion of *BUD14* in *lte1*Δ *spo12*Δ cells causes a more pronounced growth rescue phenotype
259 (Figure 3E). Deletion of *KEL2* however does not rescue *lte1*Δ *spo12*Δ lethality, while it only
260 has a minor impact on cold sensitivity of *lte1*Δ cells (Figure 3D-E). These data agree with
261 previous reports that Kel1 and Kel2 have a mitotic exit inhibitory function (Geymonat *et al*,
262 2010; Hofken & Schiebel, 2002; Seshan *et al.*, 2002) and suggest that this function of Kel1 and
263 Kel2 in mitotic exit inhibition differs from that of Bud14 as Kel1/Kel2 are not influencing the
264 SPOC.

265 **Bud14 inhibits mitotic exit through its interaction with Glc7**

266 Bud14 is a regulatory subunit of the type I Protein phosphatase (PP1) Glc7 (Cullen & Sprague,
267 2002; Knaus *et al*, 2005; Lenssen *et al*, 2005). We next asked whether Bud14 exerts its mitotic
268 exit inhibitory role through Glc7. To address this question, we used mutants with impaired
269 Glc7-Bud14 function. First, we used a mutant version of Bud14 that cannot bind Gcl7 (*bud14-*
270 *F379A*) (Knaus *et al.*, 2005) (Figure 3- Figure Supplement 1). Introduction of the wild type
271 *BUD14* but not the *bud14-F379A* mutant on a centromeric plasmid restored cold sensitivity of
272 the *lte1*Δ *bud14*Δ (Figure 4A). Likewise, expression of *BUD14* but not *bud14-F379A* on a
273 centromeric plasmid under *BUD14* endogenous/native promoter rescued the SPOC deficient
274 phenotype of *bud14*Δ *kar9*Δ cells (Figure 4B). These data suggests that Glc7-Bud14 interaction
275 is essential for Bud14 function in SPOC.

276 Next, we used the temperature sensitive *glc7-12* mutant (Andrews & Stark, 2000; Cheng &
277 Chen, 2010) to further confirm the contribution of Glc7 to mitotic exit inhibition. *glc7-12*
278 exhibits a growth defect at 33-35 ºC and is lethal at 37 ºC, as an indication of Glc7 partial and
279 full inactivation at these temperatures respectively (Figure 4 - Supplement 1A, YPD plates)
280 (Andrews & Stark, 2000; Cheng & Chen, 2010). Partial inactivation of *glc7-12* at 33-35 ºC is
281 also evident when examining other phenotypes attributed to Glc7 deficiency (Andrews &
282 Stark, 2000; Cheng & Chen, 2010), such as sensitivity to hydroxyurea (Figure 4 – Figure
283 Supplement 1A, HU plates) and accumulation of large-budded cells with single nucleus (Figure
284 4 – Figure Supplement 1B). At 18 ºC, which is a permissive temperature for *glc7-12, glc7-12*
285 *lte1Δ spo12Δ* cells failed to form colonies (Figure 4C) replicating the lethality of *lte1Δ spo12Δ*
286 (Figure 1A). However, at the semi-permissive temperatures of *glc7-12* (33 ºC-35 ºC), *glc7-12*
287 *lte1Δ spo12Δ* cells were able to form colonies (Figure 4C). Thus, similar to the deletion of
288 *BUD14*, partial inactivation of Glc7 rescues lethality of *lte1Δ spo12Δ*. Furthermore, *glc7-12*
289 *kar9*Δ cells were SPOC deficient at 33 ºC (Figure 4D). Thus, we conclude that Glc7-Bud14
290 activity is crucial for SPOC function.

291 **Bud14 interacts with Bfa1 in the yeast two hybrid system**

292 We sought to understand the target of Bud14 among SPOC proteins. For this, we performed a
293 yeast two hybrid assay. We used Bfa1, Bub2 and Kin4 as bait proteins and Kel1 as a positive
294 control in this assay. Formation of a blue color indicates activation of the ß-galactosidase gene
295 and hence physical interaction of LexA DNA binding domain fused with Bud14 (PMM5-
296 Bud14) and Gal4-Activation Domain fused with the bait protein (pMM6-Bait protein). We
297 observed blue color formation in cells bearing pMM5-Bud14 and pMM6-Kel1 as expected due
298 to their known physical interaction (Gould *et al.*, 2014; Krogan *et al*, 2006; Neller *et al*, 2015).
299 We observed a similar interaction between Bud14 and Bfa1 but not Bub2 or Kin4 (Figure 5A).

300 We could, however, not detect an interaction between Glc7 and Bfa1, Bub2 or Kin4 in our
301 yeast two hybrid system (Figure 5 – Figure Supplement 1). Intriguingly, deletion of *BUB2* but
302 not *KIN4* ceased blue color formation in cells with pMM5-Bud14 and pMM6-Bfa1, indicating
303 that Bud14-Bfa1 interaction is dependent on the presence of Bub2 (Figure 5B).

304 We next analyzed the interaction of Bfa1 with mutant forms of Bud14. Bud14-F379A that
305 cannot bind Glc7 (Figure 3 – Figure Supplement 1B) (Knaus *et al.*, 2005), interacted with Bfa1
306 similarly to the wild-type Bud14 in our yeast two hybrid setup (Figure 5C). Bud14 formin-
307 binding mutant (Bud14-5A) also interacted with Bud14 equally well (Figure 5C). Bud14
308 contains an SH3 domain at its amino terminal (amino acids 262-318), deletion of which
309 diminishes Bud14 bud cortex localization and also interferes with Bud14-Glc7 interaction
310 (Knaus *et al.*, 2005) (Figure 3 – Figure Supplement 1A). Notably, deletion of Bud14 SH3
311 domain also caused a decrease in Bud14-Bfa1 interaction (Figure 5C). Consequently, *bud14-*
312 *SH3*Δ was SPOC deficient (Figure 3A) and rescued *lte1*Δ cold sensitivity (Figure 3B). Thus,
313 SH3 domain of Bud14 is important not only for Bud14 cortex localization but also for Bud14-
314 Glc7 and Bud14-Bfa1 interaction and hence for its function in SPOC.

315 **Bud14 limits the amount of Bfa1 at dSPBs but does not affect Bfa1 symmetry upon**
316 **spindle mispositioning**

317 So far, we showed that Bud14 has a role in SPOC through its interaction with Glc7. We also
318 showed that it interacts with Bfa1. We next asked whether Bud14-Glc7 affects Bfa1 function.
319 SPOC functionality relies on a radical change in SPB localization of Bfa1-Bub2. When the
320 spindle is properly oriented, Bfa1-Bub2 preferentially localizes to the SPB that moves to the
321 daughter cell (dSPB). Upon spindle misalignment Bfa1-Bub2 is released from dSPB, hence a
322 low level of Bfa1-Bub2 is attained at both SPBs. Thus, we analyzed the effect of Bud14 on
323 SPB localization of Bfa1-Bub2. First, we compared the SPB-bound levels of Bfa1-GFP at

324 SPBs in wild type and *bud14*Δ cells with normally aligned anaphase spindles (spindle length
325 >3µm) (Figure 6A). To our surprise, more Bfa1-GFP was localized at dSPBs in *bud14*Δ cells
326 compared to wild type cells. Importantly, increased Bfa1-GFP signal at the dSPB of *bud14*Δ
327 cells returned to wild type levels when *BUD14* was introduced in these cells on a plasmid
328 (Figure 6B). Unlike *BUD14*, Introduction of the *bud14*-F379A in *bud14*Δ cells, did not cause
329 a significant reduction in the levels of Bfa1 at the dSPB (Figure 6C). These data indicate that
330 presence of Glc7-Bud14 reduces the dSPB bound Bfa1 levels.

331 Bub2 and Tem1 localization at SPBs also depend on Bfa1 (Pereira *et al.*, 2000). Accordingly,
332 Bub2-GFP and Tem1-GFP localization at dSPB was also remarkably higher in *bud14*Δ cells
333 than wild type cells (Figure 6 – Figure Supplement 1A-B). Such increase in SPB-bound levels
334 of Bfa1-Bub2 and Tem1 was not restricted to anaphase but was also present before anaphase
335 onset (spindle length = 1,5-2 µm) (Figure 6 – Figure Supplement 1C).

336 We next asked, whether the increased Bfa1-Bub2 and Tem1 recruitment to the dSPBs observed
337 in *bud14*Δ cells may cause premature activation of the MEN in these cells. Mitotic exit is
338 preceded by SPB localization of Cdc15 and Dbf2-Mob1 (Frenz *et al*, 2000; Luca *et al*, 2001;
339 Pereira *et al*, 2002; Visintin & Amon, 2001; Yoshida & Toh-e, 2001). We assessed MEN
340 activity using the SPB bound levels of Mob1-GFP owing to its brighter fluorescence signal
341 (Caydasi *et al.*, 2012). Mob1-GFP did not prematurely localize to SPBs in *bud14*Δ cells (Figure
342 6 – Figure Supplement 2A-C). The levels of Mob1-GFP at the SPBs of *bud14*Δ cells were not
343 altered in anaphase either (Figure 6- Figure Supplement 2D-E). Thus, we conclude that despite
344 the elevated levels of Bfa1-Bub2 and Tem1 at the dSPB, MEN activity is not enhanced by
345 *BUD14* deletion in cells with normally aligned spindles.

346 We next analyzed SPB-bound Bfa1 levels in cells with misaligned anaphase spindles. Similar
347 to the situation in cells with correctly aligned spindles, *bud14*Δ *kar9*Δ cells with misoriented

348 spindles had more Bfa1-GFP at their dSPBs than *kar9*Δ cells (Figure 6 – Figure Supplement
349 1D). Thus, more Bfa1 localizes at the dSPB in the absence of Bud14 regardless of the spindle
350 position and the mitotic stage.

351 When the anaphase spindle elongates in the wrong direction, phosphorylation of Bfa1 by Kin4
352 causes dissociation of Bfa1-Bub2 from dSPB. Consequently, upon spindle mispositioning,
353 SPB localization of Bfa1-GFP changes from asymmetric (more at the dSPB than mSPB) to
354 more symmetric (similar at both SPBs). We thus asked whether *bud14*Δ cells were able to
355 change their Bfa1 localization from asymmetric to symmetric in response to spindle
356 misalignment. As a measure of signal asymmetry at SPBs, we calculated Bfa1-GFP asymmetry
357 index as the ratio of Bfa1-GFP intensity at SPBs of *kar9*Δ cells with correctly aligned and
358 misaligned anaphase spindles (Figure 6D). In response to spindle mispositioning, Bfa1-GFP
359 asymmetry was drastically reduced in *kar9*Δ cells, whereas it did not significantly change in
360 *kin4*Δ *kar9*Δ cells (Figure 6D). Similar to *kar9*Δ cells, Bfa1-GFP asymmetry was also greatly
361 decreased in *bud14*Δ *kar9*Δ cells when the spindle was mispositioned (Figure 6D). We also
362 analyzed the behavior of Bfa1-GFP through time-lapse experiments. Consistent with previous
363 reports, SPB bound levels of Bfa1-GFP in *kar9*Δ cells drastically decreased within few minutes
364 after elongation of the anaphase spindle in the wrong direction (Caydasi & Pereira, 2009)
365 (Figure 6 – Figure Supplement 3A). Bfa1-GFP also rapidly decreased at SPBs of *bud14*Δ *kar9*Δ
366 cells (Figure 6 – Figure Supplement 3B), which was not the case for *kar9*Δ *kin4*Δ cells (Figure
367 6 – Figure Supplement 3C). Thus, unlike Kin4, Bud14 does not promote a change in SPB
368 localization of Bfa1 in response to spindle mispositioning, but rather limits the levels of SPB-
369 bound Bfa1 regardless of the spindle position. These observations altogether suggest a role for
370 Bud14-Glc7 in controlling Bfa1 sequestration at the SPB in a way differently than Kin4 and
371 further support the conclusion that Kin4 and Bud14-Glc7 work in different branches of SPOC
372 activation.

373 **Glc7-Bud14 promotes Bfa1 dephosphorylation**

374 Bfa1 phosphorylation is a key regulator of mitotic exit. Cdc5 phosphorylation of Bfa1 inhibits
375 Bfa1-Bub2 GAP activity towards Tem1 to promote mitotic exit; whereas Kin4 phosphorylation
376 of Bfa1 prevents Cdc5 phosphorylation of Bfa1 to block mitotic exit (Geymonat *et al.*, 2002;
377 Hu *et al.*, 2001; Maekawa *et al.*, 2007). We asked whether Bud14 impinges on Bfa1
378 phosphorylation. To investigate Bfa1 phosphorylation, we made use of *lte1*Δ Gal1-UPL-*TEM1*
379 cells which arrest in late anaphase upon depletion of Tem1 with Kin4 localized at both SPBs
380 (Bertazzi *et al.*, 2011; Hu *et al.*, 2001). This arrest mimics a SPOC activated state where Cdc5
381 phosphorylation of Bfa1 is prevented by Kin4 phosphorylation of Bfa1 and consequently Bfa1
382 hyperphosphorylation is restored upon deletion of *KIN4* in these cells (Bertazzi *et al.*, 2011)
383 (Figure 7- Figure Supplement 1). Markedly, deletion of *BUD14* also resulted in appearance of
384 slow migrating Bfa1 forms in *lte1*Δ Gal1-UPL-*TEM1* cells (Figure 7A-B, Figure 7- Figure
385 Supplement 1B) although Kin4 was localized at both SPBs (Figure 2 – Figure Supplement 1D).
386 Such slow migrating forms of Bfa1 in *lte1*Δ *bud14*Δ cells were dependent on Cdc5 as they
387 disappeared in *cdc5-10 lte1*Δ *bud14*Δ cells arrested in anaphase (Figure 7C). These data
388 indicate that Bud14 prevents Cdc5-dependent hyperphosphorylation of Bfa1 in *lte1*Δ cells.

389 We next analyzed the effect of *BUD14* overexpression on Bfa1 phosphorylation. Bud14
390 overexpression causes cells to arrest in a pre-anaphase state and, hence, it is lethal (Chesarone
391 *et al.*, 2009; Cullen & Sprague, 2002; Knaus *et al.*, 2005; Pinsky *et al*, 2006). Of importance,
392 this lethality is not dependent on Bfa1 or Kin4 (Figure 7 – Figure Supplement 2A). To obtain
393 cells arrested in anaphase in the presence of high levels of Bud14, we first arrested *cdc15-as*
394 (L99G) (Bishop *et al*, 2000; D'Aquino *et al.*, 2005) bearing cells in anaphase through 1NM-
395 PP1 treatment and then induced Gal1-*BUD14* overexpression by addition of Galactose into the
396 growth medium. Overexpression of *BUD14* (Figure 7D) but not *bud14-F379A* caused a

397 reduction in hyperphosphorylated forms of Bfa1 (Figure 7E-F). This data suggests that Glc7-
398 Bud14 causes dephosphorylation of hyperphosphorylated Bfa1 in anaphase arrested cells.

399 To further understand whether Glc7-Bud14 dephosphorylates Bfa1, we performed an *in vitro*
400 dephosphorylation assay. For this, we enriched Bfa1-3HA from Gal1-UPL-*TEM1 kin4*Δ cells
401 arrested in telophase through depletion of Tem1 and incubated it with or without
402 immunoprecipitated Glc7-TAP in the presence or absence of 1.5 μM okadaic acid to inhibit
403 Glc7 (Bialojan & Takai, 1988; Cohen *et al*, 1989a; Cohen *et al*, 1989b) (Figure 7G). Addition
404 of Glc7-TAP in the phosphatase reaction caused a down shift of Bfa1-3HA, but not when
405 okadaic acid was added (Figure 7G). Same behavior was observed when Bud14-TAP was used
406 in the phosphatase reaction instead of Glc7-TAP (Figure 7 – Figure Supplement 2B). These
407 data altogether show that Glc7-Bud14 promotes dephosphorylation of hyperphosphorylated
408 Bfa1 in anaphase.

409

410 **Discussion**

411 SPOC is a surveillance mechanism that inhibits mitotic exit in response to spindle
412 mispositioning. Protein phosphorylation and localization play a key role in SPOC. Especially
413 the activity of Bfa1, the most downstream effector of the SPOC is tightly controlled with
414 respect to the spindle orientation through phosphorylation by the polo like kinase Cdc5 and the
415 mother specific kinase Kin4 in an opposing manner. Phosphorylation of Bfa1 in turn affects
416 activity and localization of Bfa1-Bub2 and hence the activity and the localization of the GTPase
417 Tem1 at SPBs. Despite the knowledge on Bfa1 phosphorylating kinases, knowledge on
418 phosphatases counteracting these kinases has been limited. In this study we established Glc7-
419 Bud14 as a novel SPOC component that promote dephosphorylation of Bfa1 when Bfa1 is
420 hyperphosphorylated in anaphase in a Cdc5-dependent manner. Our work supports a model
421 where Bfa1-Bub2 is activated by Glc7-Bud14 in parallel to Kin4. Upon spindle misalignment
422 in this model, the SPOC kinase Kin4 phosphorylates Bfa1 to remove Bfa1 from the SPBs,
423 away from the inhibitory kinase Cdc5, and Glc7-Bud14 dephosphorylates Bfa1 to remove its
424 inhibitory phosphorylation.

425 **Glc7-Bud14 is a SPOC component**

426 Our study identified Glc7, the budding yeast protein phosphatase 1, in association with its
427 regulatory subunit Bud14 as a novel SPOC component that inhibits mitotic exit upon spindle
428 mispositioning. Several lines of evidence led us to this conclusion. First, similar to other SPOC
429 proteins, *BUD14* deletion rescued growth of several mutants impaired in mitotic exit, including
430 the cold sensitive *lte1*Δ cells, the temperature sensitive MEN mutants (*cdc15-1*, *dbf2-2* and
431 *mob1-67*), and the synthetic lethal *lte1*Δ *spo12*Δ cells. Partial impairment of Glc7 function via
432 the *glc7-12* mutant also rescued growth lethality of *lte1*Δ *spo12*Δ cells. In addition, a Bud14
433 mutant that cannot bind Glc7 (*bud14-F379A*) (Knaus *et al.*, 2005) also rescued cold sensitivity

434 of *lte1*Δ cells. Second, similar to other SPOC proteins, *BUD14* deletion caused accumulation
435 of multinucleated cells when spindle misalignment was induced in cells by deletion of *KAR9*
436 or *DYN1*, implying that *bud14*Δ cells are deficient in arresting upon mispositioning of the
437 anaphase spindle. Of importance, similar to *bud14*Δ, *glc7-12* and the *bud14-F379A* mutants
438 were also SPOC deficient. Bud14 was implicated in the Dynein pathway of spindle positioning
439 (Knaus *et al.*, 2005). However, deletion of *BUD14* caused accumulation of multinucleated
440 phenotypes not only in *kar9*Δ but also in *dyn1*Δ backgrounds indicating that the function of
441 Bud14 in Dynein activation is not contributing to the observed multinucleation phenotype. In
442 line with this notion, time-lapse analysis revealed that *bud14*Δ *kar9*Δ cells exited mitosis
443 regardless of the spindle position. Furthermore, similar to other SPOC components, absence of
444 *BUD14* did not affect the timing of mitotic exit when the spindle was correctly positioned but
445 was crucial for delaying exit from mitosis when the spindle is misoriented. Data supporting
446 this included the anaphase duration of *bud14*Δ *kar9*Δ cells with normally positioned spindles,
447 which was not different than that of *kar9*Δ cells and also Mob1-GFP localization in *bud14*Δ
448 cells, which was not different than in wild type cells.

449 **Glc7-Bud14 works in a pathway parallel to Kin4**

450 Our data showed that Bud14 does not work in the Kin4 branch of SPOC. First, Kin4
451 localization and phosphorylation did not depend on Bud14. Second, Kin4 overexpression still
452 caused toxicity in *BUD14* deleted cells indicating that Kin4, when produced at high levels, is
453 able to keep Bfa1 active. Furthermore, time-lapse analysis of Bfa1 localization during spindle
454 misalignment showed that Bfa1 is being removed from SPBs of *bud14*Δ cells with misaligned
455 spindles, while removal of Bfa1 from SPBs is largely a Kin4 dependent process (Caydasi &
456 Pereira, 2009; Monje-Casas & Amon, 2009). Thus, Kin4 is able to exert its effect on Bfa1 in
457 the absence of *BUD14*. These data altogether exclude the possibility that Bud14 works through

458 Kin4 branch of the SPOC and suggests a model in which Glc7-Bud14 prevents mitotic exit of
459 cells with misaligned spindles in a way parallel to Kin4. In support of this model, we observed
460 an additive decrease in anaphase duration of *kin4*Δ *bud14*Δ cells with misaligned spindles
461 compared to the cells bearing single gene deletions of *KIN4* or *BUD14*. Importantly, *kin4*Δ
462 *bud14*Δ cells completely failed to delay mitotic exit while *kin4*Δ or *bud14*Δ cells were able to
463 slightly delay mitotic exit in response to spindle misorientation (Figure 2C). Accordingly,
464 SPOC activity in *kin4*Δ *bud14*Δ cells was as disrupted as in *bfa1*Δ cells (Figure 2A). Thus, we
465 propose that Kin4 and Bud14 work in parallel and presence of both is critical for a robust SPOC
466 arrest.

467 Interestingly, neither *KIN4* nor *BUD14* is required for spindle assembly checkpoint dependent
468 metaphase arrest of cells, whereas Bfa1-Bub2 is (data not shown) (Pereira & Schiebel, 2005).
469 This suggest that the Kin4 and Bud14 become important to halt mitotic exit after APC/Cdc20
470 activation at the metaphase-anaphase transition. Anaphase onset also brings about the partial
471 activation of Cdc14 by the FEAR pathway which primes MEN activation in several ways and
472 Kin4 was shown to be dispensable for SPOC in cells lacking FEAR activity (Caydasi *et al.*,
473 2017; Falk *et al*, 2016a; Scarfone *et al.*, 2015). Consistently, Bud14 was also dispensable for
474 SPOC in *spo12*Δ cells that lack FEAR (data not shown). These data support that Kin4 and
475 Bud14 work in parallel to keep Bfa1-Bub2 active in anaphase, to provide an arrest of anaphase
476 cells prior to mitotic exit.

477 **Glc7-Bud14 promotes dephosphorylation of Bfa1**

478 The SPOC component Bfa1 is a highly phosphorylated protein in a cell cycle dependent
479 manner. So far, Bfa1 has been shown to be the target of kinases Cdk1, Cdc5 and Kin4 (Caydasi
480 *et al.*, 2017; Geymonat *et al*, 2003; Hu *et al.*, 2001; Pereira & Schiebel, 2005). Among these
481 kinases Cdc5 plays an inhibitory role, whereas Cdk1 and Kin4 plays and activating role. It is

482 possible that other kinases may also phosphorylate Bfa1. There has been an ongoing curiosity
483 for phosphatases that act on Bfa1. So far, Cdc14 was shown to counteract Cdk1
484 phosphorylation of Bfa1 to partially inhibit Bfa1-Bub2 activity after anaphase onset (Caydasi
485 *et al.*, 2017) and PP2A-Cdc55 was shown to counteract Cdc5 dependent phosphorylation of
486 Bfa1 before anaphase onset, and hence downregulation of PP2A-Cdc55 activity after anaphase
487 onset facilitates Bfa1 inhibition (Baro *et al*, 2013). Our data that Bfa1 appears
488 hyperphosphorylated in *lte1*Δ *bud14*Δ cells, in a Cdc5 dependent manner, during anaphase
489 indicate that Glc7-Bud14 promotes dephosphorylation of hyperphosphorylated Bfa1 after
490 anaphase onset. Consistently, overexpression of *BUD14* but not the *bud14-F379A*, which
491 cannot bind Glc7, promoted dephosphorylation of Bfa1 in anaphase arrested cells.
492 Furthermore, through an in vitro dephosphorylation assay we showed that Glc7-Bud14 is able
493 to dephosphorylate hyperphosphorylated Bfa1 purified from anaphase arrested cells.

494 We further showed that Bfa1 and Bud14 interacted in yeast two hybrid assays. Curiously, Bfa1-
495 Bud14 interaction observed in the yeast two hybrid assay required presence of Bub2. Thus,
496 Bud14 may recognize Bfa1-Bub2 as a complex, or the interaction between Bud14 and Bfa1
497 may require *in vivo* modifications of Bfa1 that occur only when bound to Bub2. It has been
498 known that hyperphosphorylated forms of Bfa1 abolishes in the absence of Bub2 (Lee *et al*,
499 2001b). In addition, Bfa1 fails to localize to SPBs in the absence of Bub2 (Pereira *et al.*, 2000).
500 Furthermore, Bfa1 phosphorylation by Cdc5 takes place at SPBs (Maekawa *et al.*, 2007;
501 Pereira *et al.*, 2000).

502 These findings, altogether, are suggestive of a model in which Glc7-Bud14 may recognize
503 specifically a phosphorylated form of Bfa1. We favor a speculative model where Glc7-Bud14
504 dephosphorylates Cdc5-phosphorylated Bfa1 specifically upon spindle misalignment. This
505 model is also in concordance with our previous conclusion that Glc7-Bud14 works in a parallel

506 pathway to Kin4. Removal of Cdc5 dependent phosphorylation of Bfa1 by Glc7-Bud14 and
507 isolation of Bfa1 away from the inhibitory Cdc5 kinase activity by Kin4 would concertedly
508 reduce the levels of Cdc5 phosphorylated Bfa1 and thus work together to rapidly increase the
509 levels of active Bfa1-Bub2.

510 Kin4 phosphorylation of Bfa1 prevents Cdc5 phosphorylation of Bfa1 both during SPOC
511 activation (i.e. anaphase arrest of *lte1*Δ cells that mimics SPOC arrest) and during the
512 metaphase arrest upon nocodazole treatment (Bertazzi *et al.*, 2011; D'Aquino *et al.*, 2005;
513 Pereira & Schiebel, 2005). However, unlike *kin4*Δ cells, *bud14*Δ cells arrested in metaphase
514 through nocodazole treatment did not have hyperphosphorylated Bfa1 (data not shown). This
515 discrepancy between Kin4 and Glc7-Bud14 may indicate alternative scenarios: First, Glc7-
516 Bud14 may dephosphorylate sites other than those phosphorylated by Cdc5. Second, there may
517 be redundant mechanisms of Bfa1 dephosphorylation at Cdc5 phosphorylation sites that
518 especially dominate in metaphase. PP2A-Cdc55 was shown to counteract Bfa1
519 phosphorylation before anaphase onset (Baro *et al.*, 2013). Therefore, one possibility is that
520 PP2A-Cdc55 and Glc7-Bud14 may work redundantly to dephosphorylate Cdc5 phosphorylated
521 Bfa1 at different stages of the cell cycle, metaphase and anaphase respectively.

522 In addition, a truncated version of Bud14 that lacks the SH3 domain was also unable to inhibit
523 mitotic exit. This truncated Bud14 is unable to localize at the bud cortex is also unable to bind
524 Glc7 (Knaus et al., 2005) (Figure 3-Figure Supplement 1B). Our yeast two hybrid analysis also
525 revealed that Bud14-SH3Δ also have a reduced binding to Bfa1 (Figure 5C). Thus, the loss in
526 SPOC activity of the Bud14-SH3Δ can be attributed to its reduced association with Glc7 and
527 Bfa1.

528 Intriguingly, another version of Bud14, which lacks the formin regulatory motif (Bud14-5A),
529 was able to yield a stronger interaction with Glc7 in our yeast two hybrid assays (Figure 3-

530 Figure Supplement 1B). This increased association may explain why Bud14-5A provided a
531 stronger SPOC activity than the Bud14 wildtype based on SPOC functionality measurements
532 (Figure 3A).

533 **Bud14 deletion causes an increase in SPB-bound levels of Bfa1-Bub2 and Tem1**

534 We observed that cells lacking *BUD14* had more Bfa1, Bub2, and Tem1 localized at dSPB,
535 making their localization more asymmetric. The asymmetry of Bfa1 at SPBs was shown to be
536 dependent on Cdc5, as in the absence of Cdc5 activity Bfa1 localized more symmetrically to
537 SPBs (Kim *et al*, 2012). Thus, presence of more Cdc5 phosphorylated Bfa1 in *bud14*Δ cells
538 may account for increased levels of Bfa1 at the dSPB, and also Bub2 and Tem1 which bind
539 SPBs in association with Bfa1. Alternatively, Glc7-Bud14 may have other targets at the SPB
540 that might normally decrease Bfa1-Bub2 docking sites at the SPBs.

541 Studies that used versions of Bfa1 forced to bind SPBs stably (Scarfone *et al.*, 2015; Valerio-
542 Santiago & Monje-Casas, 2011), suggested that increased Bfa1-Bub2 localization at SPBs can
543 lead to increased MEN activity, as it also causes increased Tem1 association with SPBs. Does
544 altered localization of Bfa1-Bub2 and Tem1 observed in *bud14*Δ contribute to mitotic exit?
545 Analysis of Mob1 localization as a marker for MEN activation suggests that *bud14*Δ cells does
546 not activate MEN prematurely. This suggests that Bud14-Glc7 may be inhibiting mitotic exit
547 by activation of Bfa1-Bub2 GAP complex through counteracting an inactivating
548 phosphorylation of Bfa1 rather than through modulating SPB-bound levels of Bfa1-Bub2. We
549 favor that the change in SPB localization is a consequence of the change in the phosphorylation
550 status of Bfa1 or another target at the SPB.

551 **Role of PP1 through the cell cycle**

552 PP1 has numerous functions in the control of the cell cycle (Holder *et al*, 2019; Kim *et al*,
553 2016; Moura & Conde, 2019; Nasa & Kettenbach, 2018). PP1, together with PP2A, is required
554 for mitotic exit in animal cells by counteracting CDK activity (Wu *et al*, 2009). In human cells,
555 PP1 also regulates centrosome splitting by antagonizing the Nek2 kinase (Meraldi & Nigg,
556 2001). In addition, PP1 facilitates abscission by counteracting Plk1 mediated phosphorylation
557 of the centrosomal protein CEP55 during late mitosis and thus promoting its midbody
558 localization (Gao *et al*, 2018). In meiosis of Xenopus oocytes, PP1 regulates G2/M transition
559 by partially activating Cdc25 (Perdiguero & Nebreda, 2004). From yeast to mammals, PP1 is
560 essential for silencing of the spindle assembly checkpoint through stabilization of kinetochore
561 microtubule interactions by counteracting Aurora B and by potentially regulating recruitment
562 of MCC to kinetochores (Kelly & Funabiki, 2009; Kotwaliwale & Biggins, 2006; Musacchio
563 & Salmon, 2007; Ruchaud *et al*, 2007). In this study, we show that the budding yeast PP1,
564 Glc7, in association with its regulatory subunit Bud14, inhibits mitotic exit upon anaphase
565 spindle mispositioning. This function of PP1 seems to be opposite to the mitotic exit promoting
566 role of PP1 reported in animal cells. The fact that mitotic exit is achieved by the Cdc14
567 phosphatase in budding yeast, instead of the PP1 and PP2 phosphatases (Manzano-Lopez &
568 Monje-Casas, 2020) is likely the reason for Glc7 gaining a different function after the anaphase
569 onset during the narrow time window until exit from mitosis.

570 Glc7-Bud14 was implicated in microtubule cortex interactions. Data based on Kin4 activity on
571 Bfa1 indicates that SPOC mechanism may sense microtubule-cortex interactions (Caydasi &
572 Pereira, 2009; Maekawa *et al.*, 2007; Monje-Casas & Amon, 2009; Pereira & Schiebel, 2005).
573 How spindle alignment is sensed, and this information activates SPOC still remain unknown.
574 Due to their known function in regulating microtubule-cortex interactions (Knaus *et al.*, 2005),
575 Glc7-Bud14 constitutes a great candidate for sensing of such interactions. Considering that
576 Glc7 (PP1) is a conserved phosphatase, similar mechanisms may be employed by higher

577 eukaryotes. Future work will show whether Glc7-Bud14 may act as a sensor that translates the

578 unattached microtubule-cortex interactions to the downstream SPOC machinery.

579 **Materials Methods**

580 **Yeast methods, strains and growth**

581 All yeast strains used are isogenic with S288C and are listed in Table 1. Basic yeast methods
582 and growth media were as described (Sherman, 1991). Carbon source is glucose unless
583 otherwise stated. When necessary 2% D-Raffinose, 3% D(+)-Galactose was used instead of
584 glucose. Yeast strains were grown at 30 ºC and in rich medium unless otherwise stated. Plasmid
585 containing strains were grown in synthetic complete (SC) media lacking the appropriate
586 auxotrophic nutrients. The temperature sensitive mutants and *kar9*Δ cells were maintained at
587 23 ºC. Cassette PCR-based gene editing method was used for chromosomal gene deletion and
588 C-terminal or N-terminal tagging (Janke *et al*, 2004; Knop *et al*, 1999). To determine genetic
589 interactions based on growth, mutant yeast strains bearing the wild type gene on a *URA3*-based
590 plasmid (pRS316) were spotted on 5-Fluoroorotic acid (5FOA) plates. 5FOA plates negatively
591 selects for the *URA3*-based plasmid and allows for observation of the growth phenotype in the
592 absence of the corresponding plasmid. Most *kar9*Δ cells were maintained complemented with
593 *KAR9* on *URA3-based* centromeric plasmid (pGW399), and stroke on 5FOA plates to induce
594 plasmid lost shortly before experiments on SPOC analysis. Similarly, MEN-ts mutants were
595 maintained complemented with plasmids carrying the wildtype version of the corresponding
596 MEN gene. The plasmids used in this study are listed in Table 2.

597 **Cell growth comparison on agar plates**

598 Yeast cultures were grown in appropriate media and growth conditions for 24 hours. The OD_{600}
599 of the cultures were adjusted to 1 and 10-fold serial dilutions were made using sterile PBS. 10
600 µl of serial dilutions were spotted on appropriate agar plates and grown at appropriate
601 temperatures for 1-3 days.

602 **Cell cycle synchronizations**

603 Cells were synchronized in G1 phase by treating log-phase cultures with 10 µg/ml α-factor
604 (Sigma #T6901) dissolved in DMSO and incubating for one and a half doubling time. For
605 synchronization in metaphase without spindles, 15 µg/ml nocodazole (Sigma #M1404)
606 dissolved in DMSO were added to log-phase cultures and incubated for ~2h. The arrest was
607 confirmed by microscopy after fixing the cells with 70% Ethanol and re-suspending in PBS
608 containing 1 µg/ml 4',6-diamino-2-phenylindole (DAPI, Sigma). For nocodazole arrest from
609 G1 synchronized yeast cultures, cells were first treated with α-factor and released in
610 nocodazole containing YPAD. For telophase arrest of Gal1-UPL-Tem1 bearing cells, after
611 cultures were grown to log-phase in Raffinose-Galactose containing medium, cells were
612 transferred into YPAD medium and grown for ~3 h until cells (>%90) were arrested with large
613 buds and separated nuclei. For telophase arrest from G1 arrested cells: Log-phase cultures of
614 Gal1-UPL-Tem1 bearing cells grown in Raffinose/Galactose were treated with α-factor. 30
615 min before G1 synchronization was completed, glucose was added to the culture to give 2%
616 final concentration. Then cells were released from α-factor in YPAD. The arrest was confirmed
617 by microscopy after ethanol fixation of the cells and staining the nucleus with DAPI. As for
618 anaphase arrest using *cdc15-as*, log phase cell cultures grown in YP-Raffinose medium, were
619 treated with 1NM-PP1 (2.5 µM) and incubated for 3 h. Synchronization was judged based on
620 microscopy after DAPI staining. Anaphase synchronization of *cdc5-10* cells were achieved by
621 arresting the cells in G1 at 23 ºC first and then releasing them in pre-warmed alpha factor free
622 medium at 30 ºC and incubating them at 30 ºC for 1.5 h.

623 **Microscopy Methods**

624 All fluorescence microscopy methods were performed using Carl ZEISS Axio Observer 7
625 motorized inverted epifluorescence microscope equipped with Colibri 7 LED light source,

626 Axiocam 702 Monochrome camera, 100X and 63X Plan Apochromat immersion oil objective
627 lenses, Filter sets 95 (GFP/Cherry), 20 (Rhodamin), FITC and DAPI, and an XL incubation
628 and climate chamber. For Kin4-GFP, GFP-Tubulin and Bud14-GFP analysis 63X objective
629 was used. For analysis of Bfa1-GFP, Bub2-GFP, Tem1-GFP and Mob1-GFP 100X objective
630 was used.

631 For end-point analysis of samples, wet mounts of samples were prepared by sandwiching 2 µl
632 of culture between the coverslip and slide. Cells were either fixed using 70% Ethanol and
633 stained with DAPI (for SPOC assays and mitotic index analysis) or analyzed live (For GFP
634 signal quantification). For time-lapse experiments, cells were prepared on glass bottom petri
635 dishes (WVR 10810-054 Matsunami) as described (Caydasi & Pereira, 2017). Briefly, the
636 glass center of the petri dish was covered with 6% Concanavalin A (*Canavalia ensiformis* Jack
637 Bean, type IV Sigma C2010-G). Excess Concanavalin A was washed out and 150 µl of culture
638 was pipetted on the dish followed by a 30 min incubation at 30 °C. Then, cells were aspirated
639 gently and cells that were not attached on the dish were washed out with pre-warmed fresh
640 media. After the final wash, the dish was filled with media and taken to the microscope stage
641 in the preheated chamber, equilibrated there for at least 1 hour before the start of the time-
642 lapse.

643 **SPOC functionality assays**

644 For end point analysis of SPOC functionality, log-phase *kar9*Δ cells cultured at 23°C were
645 incubated at 30°C for 3-5 h or log-phase *dyn1*Δ cells cultured at 30 °C were incubated at 18 °C
646 overnight. Cells were fixed using 70% Ethanol, re-suspended in PBS containing 1 µg/ml DAPI
647 and analyzed by microscopy. Cells bearing normal and misaligned nuclei, and cells with
648 SPOC-deficient phenotypes including multinucleated cells were counted. SPOC deficiency
649 index was calculated as:

650 $= \%\ Cells\ with\ multinucleation\ \div\ \%\ cells\ with\ mispositioned\ nuclei\ \times\ 10$

651 For time lapse analysis of SPOC functionality, GFP-Tubulin bearing *kar9*Δ cells were imaged
652 every minute for 90 min at 30 °C. 10 z-stacks of 0.4 µm thickness were taken at each time
653 point. Anaphase duration of cells with correct and misaligned spindles was calculated as the
654 time from the start of fast spindle elongation (metaphase-to-anaphase transition) until spindle
655 breakdown (Caydasi *et al.*, 2010b; Straight *et al*, 1997). Dot plots were prepared in GraphPad
656 Prism 8.0.1 (GraphPad, La Jolla, CA).

657 **Localization based fluorescence image quantifications**

658 For signal intensity quantification of Bfa1-GFP, Bub2-GFP, Tem1-GFP and Mob1-GFP, we
659 took still images of live cells bearing *SPC42*-eqFP and mCherry-*TUB1* as a mitotic marker.
660 Each still image consisted of 13 z-stacks of 0.3 µm thickness. Z-stacks of the images were sum-
661 projected, and mean fluorescence intensities were measured using Image J (NIH) software and
662 corrected as described (Caydasi *et al.*, 2012). Briefly, a 0.577 μm^2 (42 pixels) box was selected
663 around the spindle pole body under inspection (ROI, region of interest) and the mean
664 fluorescence intensity of the GFP signal was measured. Background fluorescence intensity was
665 determined by measuring an area inside the cytoplasm of respective cell, near to the region of
666 interest. The correction was done by subtracting the mean fluorescence intensity of the
667 background from the mean fluorescence intensity of the ROI.

668 To detect the behavior of asymmetric localization of Bfa1 at SPBs, ratio of the corrected signal
669 intensities (as described above) at the SPBs were calculated. For cells with normally aligned
670 spindles, the signal intensity at the dSPB was divided to the signal intensity at the mSPB. For
671 cells with misaligned spindles, the SPB with the greater signal was considered as dSPB.

672 Statistical results and graphs were computed and plotted by using Prism 8.0.1 (GraphPad, La
673 Jolla, CA). Two-tailed t-test were applied to compare the statistical significance of the signal
674 intensity measurements in a pair-wise manner. Chi-square test were applied for comparison of
675 Bud14-GFP cortex localization.

676 **Yeast Two Hybrid Assay**

677 Yeast Two Hybrid analysis was performed as described (Meitinger *et al*, 2014). Briefly,
678 indicated genes cloned into pMM5 or pEG202 (LexA-myc fusion, *HIS* autotrophy marker) and
679 pMM6 (Gal4-HA fusion, *LEU2* autotrophy marker) were transformed into the yeast strain
680 SGY37-VIII,3 that contains a chromosomally integrated LexA(op)-LacZ reporter for
681 activation of the ß-galactosidase gene. Transformants were selected on SC-His-Leu agar plates,
682 grown in SC-His-Leu media until stationary phase, diluted to 1 OD_{600} and 10 µl of each were
683 spotted on SC-His-Leu agar plates. Cells were grown for~ 48 hours and plates were overlaid
684 with 0.4% soft-agar solution containing 0.4 mg/ml X-Gal, 0.1% SDS, 10 mM KCl and 1 mM
685 $MgCl_2$. Blue color formation was monitored. Plates were scanned.

686 **Glc7 Functionality Assay**

687 For the analysis of *GLC7* functionality, *GLC7* and *glc7-12* cells were grown at 23 °C until log-
688 phase. Log-phase cultures were diluted to a OD600 value of 0.1 and shifted to 30 °C, 33 °C,
689 35 °C and 37 °C. After incubation at these temperature for 4 h cells were fixed using 70%
690 Ethanol, and then resuspended in with 1 µg/ml DAPI in 1X PBS prior to microscopic
691 visualization. Then, the cells were analyzed under fluorescence microscopy. All the cells were
692 counted and categorized according to their bud size and nucleus number. For analyzing the
693 functionality of *GLC7* by growth assay, the cultures were grown at 23 °C for 24-48 hours.
694 OD600 value of all the yeast cultures, then, was adjusted to 1.0 using 1X sterile PBS. The
695 cultures were serially diluted 10-fold using sterile 1X PBS. 7.5 µl of each serial dilutions were

696 spotted on the appropriate agar plates (YPD and YPD containing 0.01M HU). The plates were
697 incubated at the appropriate temperatures for 2-3 days.

698 **Protein Methods**

699 Total yeast protein precipitation, sample preparation, and Western blotting following Laemmli
700 SDS-PAGE were performed as previously described (Meitinger *et al*, 2016). Total cell native
701 protein extracts were prepared by lysis of cells using acid washed glass beads (Sigma) in a
702 cooling bead beater homogenizer (Analytik Jena, SpeedMill Plus). Primary antibodies were
703 Mouse-anti-HA (Gift from Gislene Pereira), Rabbit anti-Clb2 (Gift from Gislene Pereira),
704 Rabbit-anti-Tubulin (Abcam EPR13799), Rabbit anti-TAP (Thermofisher scientific
705 CAB1001) and Rabbit anti-GFP (Abcam ab290). Secondary antibodies were Goat-anti-rabbit
706 (Advansta #R-05062-500) or Goat-anti-mouse (Advansta #R-05071-500) horse radish
707 peroxidase (HRP) conjugated secondary antibodies.

708 **Phosphatase Assay**

709 Glc7-TAP and Bud14-TAP were enriched from yeast lysates on IgG Sepharose beads (GE
710 Healthcare BioScience) according to manufacturer's recommendations. In addition, ESM356-
711 1 (a strain without TAP tag) lysates were incubated with IgG Sepharose beads as a no-tag
712 control. Briefly, cell pellets of logarithmically growing cultures were lysed using acid washed
713 glass beads (Sigma) in a lysis buffer containing 50mM Hepes pH:7.5, 150mM NaCl, 1mM
714 EDTA , %1 SDS, 1mM DTT, 2mM PMSF and complete Protease Inhibitor Coctail (Roche).
715 The lysate was cleared by centrifugation at 10000 rpm at + 4 ºC and the supernatant was
716 incubated with IgG beads for 2 h at 4 ºC. Beads were washed with ice cold wash buffer
717 containing 50mM Hepes pH: 7.5, 150mM NaCl, 0.1mM EDTA, %0.1 SDS, %0.025 Tween
718 20, 1mM DTT and were immediately used for the phosphatase reaction as the phosphatase
719 source.

720 Bfa1-3HA was purified from *BFA1-3HA kin4Δ Gal1 -UPL-TEM1* cells arrested in anaphase.
721 For this, log-phase culture grown in Raffinose/Galactose containing rich medium were
722 transferred into YPAD medium. After >90% of the cell arrest was achieved, cell pellets were
723 lysed using acid washed glass beads in bead beater. Lysis buffer composition was: 50mM
724 Hepes pH:7.5, 150mM NaCl, 5% Glycerol, 1mM EDTA, 1% NP-40, 160mM β-
725 Glycerophosphate, 2mM $NaVO_3$, 100mM NaF, 2mM PMSF, 4mM Benzamidine and complete
726 Protease Inhibitor Coctail (Roche). After clearing the cell lysate by centrifugation at 10000
727 rpm at + 4 ºC, the cell extract was incubated with anti-HA magnetic beads (Thermofisher,
728 Pierce™) for 2 h at 4 ºC. After the incubation the beads were washed in 50mM Hepes pH: 7.5,
729 150mM NaCl, %1 NP-40, %5 Glycerol, 1mM EDTA and eluted from beads under basic elution
730 conditions according to manufacturer's protocol. Briefly, beads were incubated with 50mM
731 NaOH for 5 minutes and the eluate was immediately neutralized by 300mM Tris pH:8.5. Next,
732 the eluate was applied on PD MiniTrap G-25 Sephadex (GE Healthcare) columns equilibrated
733 with a buffer containing 50mM Hepes pH: 7.5, 100mM NaCl. Buffer exchange was performed
734 according to manufacturer's spin protocol.

735 In vitro phosphatase reaction was performed using the IgG-beads that contained Bud14-TAP
736 or Glc7-TAP or the IgG-beads that was incubated with the cell extract of the ESM356-1
737 control. Bfa1-3HA that was prepared as explained above was added as the substrate.
738 Phosphatase reaction buffer composition was 100mM NaCl, 50mM Hepes pH: 7.5, 2mM DTT,
739 %0.025 Tween, 2mM $MnCl_2$. Okadaic acid (Abcam) was also added to the indicated reactions
740 to 1.5 µM final concentration. After reaction was incubated at 30 ºC for 1h, 5x sample buffer
741 was added immediately into the reaction tubes, samples were boiled at 95 ºC for 5 min and
742 analyzed by western blotting.

743 **Quantification of hyperphosphorylation of Bfa1**

744 Bfa1-3HA containing protein samples were run 8% Laemmli SDS-PAGE gels, for about 3-3.5
745 hours. The gel tank was placed in an ice-filled bucked during running. Gels were run at 50V
746 for about 30 min (to allow passage of proteins from stacking to separating gel), and at 100V
747 for the remaining time. Semi-dry blotting was performed for 2h at 0.1 A per gel and signals
748 were detected on x-ray films using ECL. X-ray films were scanned, and the images were
749 analyzed in Image J. Mean grey value of the top half and bottom half of the Bfa1-3HA bands
750 at each line was quantified using Image J measure tool. The area sizes were kept constant for
751 each blot. Background mean intensity of the film was also quantified and subtracted from that
752 of the measured Bfa1-3HA band intensities for correction. Corrected intensity of the top half
753 was divided to the corrected intensity of the bottom half of the Bfa1-3HA bands and the values
754 were plotted.

Acknowledgements

This work was supported by TÜBITAK Grant No. 117C041. Work of AKC was supported by EMBO installation Grant No. 3918 and ICGEB installation Grant No. CRP/TUR17-04_EC. CD was funded by Koç University, HK and IK were funded by TÜBITAK Grant No. 118Z979 and SNE was funded by TÜBITAK Grant No. 117Z232 granted to AKC. AKC was funded by MSCA Individual Fellowship No. 796599-COHEMEX. We are grateful to Gislene Pereira (COS, Heidelberg), Elmar Schiebel (ZMBH, Heidelberg), Claudio De Virgilio (University of Fribourg, Fribourg), Matthias Peter (ETH, Zürich) and Michael Knop (ZMBH, Heidelberg) for sharing reagents, strains and plasmids.

Author Contributions

HK, DK, CD, IK and SNE designed and performed the experiments. AKC acquired funding, designed experiments, supervised HK, DK, CD, IK, SNE, and wrote the manuscript.

Conflict of Interest

The authors declare that they have no conflict of interest.

770 **Figure Legends**

771 **Figure 1. Bud14 deletion rescues growth of cells with impaired mitotic exit. A.** *bud14*Δ
772 cells rescue the synthetic lethality of *lte1*Δ *spo12*Δ cells. **B.** *bud14*Δ cells rescue the lethality
773 of *lte1*Δ cells at 18 ºC. **C.** Comparison of growth rescue of MEN-ts mutants upon deletion of
774 *BUD14* and *BFA1*. Serial dilutions of indicated strains were spotted on indicated plates and
775 grown at given temperatures. 5-FOA plates negatively selects for the *URA3*-based plasmids
776 (pRS316 containing the *LTE1* in A and B, pRS316 containing the wild type gene copy of the
777 corresponding MEN mutant in C. Thus, only cells that have lost these plasmids can grow on
778 5-FOA plates where genetic interactions can be observed.

779 **Figure 2. *bud14*Δ cells are SPOC deficient. A-B.** End-point analysis of SPOC integrity of
780 indicated yeast strains in *kar9*Δ (A) and *dyn1*Δ (B) background. Cells were fixed with ethanol
781 and stained with DAPI. Cells with normally aligned nuclei, mispositioned nuclei and multi
782 nucleated cells that failed to correctly position their spindle before mitotic exit were counted
783 by microscopy and their SPOC deficiency index percentages were plotted, where SPOC
784 deficiency index = % cells with multinucleation ÷ % cells with mispositioned nuclei x 10.
785 Graphs are average of three independent experiments. A minimum of 100 cells were counted
786 from each strain in each experiment. Error bars show standard deviation. Two-tailed Student's
787 t-test was applied. ** $p < 0.01$, *** $p < 0.001$. **C.** Single cell analysis of SPOC integrity in
788 indicated strains. Duration of anaphase in cells with misaligned and normally aligned spindles
789 were calculated as explained in the text and plotted as dot-plots. Data points in red indicate the
790 cells in which the spindle did not break down during the time lapse movie. In this case, plotted
791 values are the time duration during which these cells were observed in anaphase through the
792 time lapse movie. Consequently, the actual anaphase duration is greater than the value plotted
793 in red. This fact is emphasized in the red part of the y-axis, indicated above the red dashed line,

794 with addition of the “>” symbol before the y-axis values. Green dash line indicates the mean
795 value of the anaphase duration in cells with normally aligned spindles. One-way Anova with
796 uncorrected Fisher’s LSD was applied for statistical analysis. *** $p < 0.001$, **** $p < 0.0001$
797 n: sample size. All pairwise comparisons and descriptive statistics are shown in the
798 corresponding source data file, whereas only comparisons of normal and misaligned spindles
799 are shown in the figure.

800 **Figure 3. Function of Bud14 in actin regulation is dispensable for SPOC. A.** End-point
801 analysis of SPOC deficiency index in *bud14*Δ *kar9*Δ cells carrying *URA3-based* empty plasmid
802 (empty) or *BUD14*-containing *URA3*-based plasmids (*BUD14, bud14-5A* and *bud14-ΔSH3*).
803 Graphs are average of three independent experiments. A minimum of 100 cells were counted
804 from each strain in each experiment. Error bars show standard deviation. *$p<0.05$ according to
805 Student’s t-test. **B.** Serial dilutions of indicated strains bearing *URA3-based* empty plasmid
806 (not indicated on figure) or *BUD14*-containing *URA3*-based plasmids (*BUD14, bud14-5A* and
807 *bud14-ΔSH3*) were spotted on SC-URA plate and grown at indicated temperatures. **C.** End-
808 point analysis of SPOC deficiency index in indicated cell types. Graphs are average of three
809 independent experiments. A minimum of 100 cells were counted from each strain in each
810 experiment. Error bars show standard deviation. ***$p<0.001$ according to Student’s t-test. **D-**
811 **E.** Serial dilutions of indicated strains bearing *LTE1* on *URA3*-based pRS316 plasmid were
812 spotted on 5-FOA and SC plates and grown at indicated temperatures. 5-FOA negatively
813 selects for *URA3* containing plasmids, thus cells lose their pRS316-*LTE1* plasmids on 5-FOA
814 plates and genetic interactions can be observed on this plate.

815 **Figure 4. Glc7-Bud14 interaction is required for SPOC regulatory function of Bud14. A.**
816 Serial dilutions of indicated strains bearing *URA3*-based empty plasmid (not indicated on
817 figure) or *BUD14*-containing *URA3*-based plasmids (*BUD14* and *bud14-F379A*) were spotted

818 on SC-URA plate and grown at indicated temperatures. **B.** SPOC deficiency indexes of
819 indicated strains carrying *URA3*-based empty plasmid (empty) or *BUD14*-containing *URA3*-
820 based plasmids (*BUD14* and *bud14-F379A*). Graphs are average of three independent
821 experiments. A minimum of 100 cells were counted from each strain in each experiment. Error
822 bars show standard deviation. * $p<0.05$ according to student's t-test. **C.** Serial dilutions of
823 indicated strains were spotted on 5-FOA plate and grown at indicated temperatures. Cells that
824 contain *LTE1* on a *URA3* based plasmid are indicated with *pRS316-LTE1*. **D.** SPOC deficiency
825 indexes of indicated strains. *$p< 0.05$ according to student's t-test.
826
827 **Figure 5. Yeast two hybrid analysis of Bud14 and Bud14 mutants with SPOC proteins.**
828 **A.** Bud14 interacts with Bfa1 but not with Bub2 or Kin4. **B.** Bud14-Bfa1 interaction is
829 dependent on Bub2. **C.** Bfa1-Bud14 interaction is reduced in Bud14ΔSH3 mutant. SGY37 was
830 co-transformed with indicated plasmids. Empty plasmids served as a control for any self-
831 activation. Kel1 served as a positive control. Cells were grown for two days on selective agar
832 plates before overlay. Blue color formation was monitored as an indication of protein-protein
833 interaction.

834 **Figure 6. More Bfa1 localizes to dSPB in the absence of *BUD14*. A.** Bfa1-GFP signal
835 intensity quantifications at the SPBs of *BFA1-GFP mCherry-TUB1 or BFA1-GFP mCherry-*
836 *TUB1 bud14*Δ cells with normal aligned anaphase spindles were plotted on the right. Black
837 and grey lines in the dot plots are the mean value and standard deviation respectively.
838 Representative still images of cells were shown on the left. **B.** Bfa1-GFP signal intensities at
839 the dSPB were plotted in *BUD14* and *bud14*Δ cells bearing empty plasmid (blue and red), as
840 well as *bud14*Δ cells bearing a ADH-*BUD14* containing plasmid (green). **C.** Bfa1-GFP signal
841 intensities at the dSPB were plotted in *bud14*Δ *cells* bearing empty plasmid (red), ADH1-
842 *BUD14* containing plasmid (green) and ADH1-*bud14-F379A* containing plasmid (yellow) **D.**

843 Analysis of Bfa1-GFP asymmetry at the SPBs of *kar9*Δ, *kar9*Δ *kin4*Δ and *kar9*Δ *bud14*Δ cells
844 with correctly aligned and misaligned anaphase spindles. Box and Whisker plot shows the ratio
845 of Bfa1-GFP signal intensities at the SPB1 and SPB2, where SPB1 always corresponds to SPB
846 with the greater Bfa1-GFP signal. The box represents first and third quartile while the whiskers
847 show 10-90 percentile of the data. The horizontal line in the box indicates the median of the
848 data. Only comparisons of normal and misaligned spindles are shown in the figure.
849 Representative still images of cells are shown on the right. n: sample size. Scale bar: 2 µm.
850 One-way Anova with uncorrected Fisher's LSD was applied for all statistical analysis. **
851 $p<0.01$, *** $p < 0.001$, **** $p < 0.0001$. All pairwise comparisons are shown in the
852 corresponding source data file.

853 **Figure 7. Glc7-Bud14 promotes Bfa1 dephosphorylation in anaphase. A.** Bfa1-3HA Gal1-
854 UPL-Tem1 containing *lte1*Δ and *lte1*Δ*bud14*Δ cells grown in galactose containing medium
855 were released from alpha factor imposed G1 arrest (t=0) into an alpha factor free medium
856 supplemented with glucose to achieve Tem1 depletion and samples were collected at indicated
857 time points. Bfa1-3HA mobility shift was analyzed via western blotting using anti-HA
858 antibodies. Red arrow indicates hyperphosphorylated forms of Bfa1-3HA whereas blue arrow
859 indicates hypophosphorylated forms of Bfa1-3HA. Percentage of cells with single nucleus (1
860 DAPI) and two separate nuclei (2 DAPI) were plotted as a marker for cell cycle progression.
861 **B.** Indicated time points of each cell type from the experiment shown in A were loaded side-
862 by-side for better comparison of Bfa1-3HA mobility. **C.** Bfa1-3HA mobility in Gal1-UPL-
863 Tem1 or *cdc5-10* bearing *LTE1 BUD14* or *lte1*Δ*bud14*Δ cells. Percentage of cells with two
864 separate nuclei (% 2DAPI) were indicated as a measure of cells in anaphase. *C*ells were first
865 arrested in G1, then released from the G1 arrest and cultured for 90 min before sample
866 collection. Gal1-UPL-Tem1 cells were treated as in A to achieve the anaphase arrest, whereas
867 anaphase arrest of *cdc5-10* cells was achieved through growth at 37 ºC. **D.** *cdc15-as* bearing

868 cells bearing *BUD14* or Gal1-*BUD14* at the Bud14 endogenous locus were grown to log-phase
869 in raffinose containing medium, treated with 1NM-PP1 for 2,5h followed by galactose addition
870 (t0) to the medium. Samples were collected at 0h, 2h and 3h after galactose addition and Bfa1
871 mobility was analyzed. Percentage of cells with two separate nuclei (% 2DAPI) were indicated
872 as a measure of cells in anaphase. **E.** *cdc15-as bud14*Δ cells with *BUD14*-9myc, Gal1-*BUD14*-
873 9myc, or Gal1-*bud14-F379A*-9myc integrated at the chromosomal *leu2* locus were grown to
874 log-phase in raffinose containing medium, treated with 1NM-PP1 for 3h, followed by galactose
875 addition (t0) to the medium. Samples were collected at 0h, 1h, 2h and 3h after galactose
876 addition and Bfa1 mobility was analyzed. Percentage of cells with two separate nuclei (%
877 2DAPI) were indicated as a measure of cells in anaphase. **F**. Quantification of relative levels
878 of hypersphosphorylated Bfa1 from the experiment shown in E. Band intensity ratio of slow
879 migrating forms to fast migrating forms of Bfa1 was plotted. **G.** In vitro phosphatase assay of
880 immunoprecipitated Glc7-TAP on IgG beads were incubated with Bfa1-3HA purified from
881 *BFA1-3HA* Gal1-UPL-TEM1 *kin4*Δ cells in the presence or absence of 1.5 μM Okadaic acid.
882 As a no Glc7-TAP control, IgG beads incubated with cell lysates of ESM356-1 were used.
883 Glc7-TAP levels were detected using anti-TAP antibodies. Bfa1-3HA was detected using anti-
884 HA antibodies. Red and blue arrows indicate slow migrating and fast migrating forms of Bfa1-
885 3HA respectively. Quantification of relative levels of hypersphosphorylated Bfa1 is shown on
886 the right. Each color represents a different independent experiment. One-way Anova with
887 uncorrected Fisher's LSD was applied for statistical analysis. ** $p<0.01$, **** $p < 0.0001$.

888

889 **Supplementary Figure Legends**

890 **Figure 2 – Figure Supplement 1. Bud14 does not influence Kin4 function. A.** Serial
891 dilutions of indicated strains were spotted on Glucose containing (YPD) and Galactose
892 containing (YP Raf/Gal) agar plates. Gal1-Kin4 overexpression is induced on Galactose
893 containing plates. **B.** Logarithmic growing cultures bearing Kin4-GFP and Spc42-eqFP were
894 treated with nocodazole for 2 hours and Kin4 SPB and cortex localization was analyzed by
895 microscopy. *rts1*Δ cells were used as a control in which Kin4 fails to localize to SPBs and
896 cortex. Graph is an average of three independent experiments. Error bars are standard
897 deviation. At least 100 cells were counted from each sample in each experiment. Scale bar: 2
898 µm. **C.** SPB localization of Kin4-GFP was analyzed in logarithmic growing *lte1*Δ and *lte1*Δ
899 *bud14*Δ cultures. Spc42-eqFP and mCherry-Tub1 served as SPB and spindle markers. Only
900 cells in anaphase were considered. Graphs were plotted as described in (B). **D.** Logarithmic
901 growing cultures bearing Kin4-6HA and the indicated gene deletions were treated with
902 nocodazole for 2.5 h. Kin4 mobility shift was analyzed by western blotting using anti-HA
903 antibodies. *rts1*Δ served as a control for hyperphosphorylated Kin4.

904 **Figure 3 - Figure Supplement 1. Expression and Glc7 binding of Bud14 mutants. A.**
905 Analysis of *BUD14* expression in cells bearing pMK60 (*pRS416-endogenous-BUD14-*
906 *promoter-GFP-BUD14*), pDKY001 (*pRS416-endogenous-BUD14-promoter-GFP*-bud14^{5A}),
907 pHK002 (*pRS416-endogenous-BUD14-promoter-GFP-bud14-F379A*), pDKY003 (*pRS416-*
908 *endogenous-BUD14-promoter-GFP-bud14-ΔSH3*) Bud14 was detected using anti-GFP
909 antibodies. **B.** Interaction of Glc7 with Bud14 and Bud14 mutants in yeast two hybrid system.

910 **Figure 4 – Figure Supplement 1. Assessment of *glc7-12* inactivation at different**
911 **temperatures. A.** Serial dilutions of indicated strains were spotted on YPD and YPD
912 containing 0.01M HU and grown at indicated temperatures. The plates then were incubated at

913 given temperatures for 2-3 days. **B.** Analysis of cell morphology of *GLC7* and *glc7-12* cells at
914 indicated temperatures. Liquid cultures were grown to log-phase at 23 ºC, shifted to indicated
915 temperatures and further grown for 4 h. Cells were fixed with ethanol and stained with DAPI.
916 Cells were counted by microscopy and percentages of cells with large buds and single DAPI
917 were plotted. A minimum of 100 cells were counted from each strain.
918
919 **Figure 5 - Figure Supplement 1. Analysis of Glc7 interaction with SPOC components. A.**
920 Yeast two hybrid assays of Glc7 with Bfa1, Bub2 and Kin4. Bud14 was included as a positive
921 control.

922 **Figure 6 - Figure Supplement 1. Bfa1, Bub2 and Tem1 localization in *bud14*Δ cells during**
923 **anaphase and metaphase. A-B.** Bub2-GFP and Tem1-GFP representative images (A) and
924 signal intensity quantifications at the SPBs (B) of *BFA1-GFP mCherry-TUB1* or *BFA1-GFP*
925 *mCherry-TUB1 bud14*Δ cells with normal aligned anaphase spindles. Black and grey lines in
926 the dot plots are the mean value and standard deviation respectively. Representative still images
927 of cells were shown in A. **C.** Bfa1-GFP, Bub2-GFP and Tem1-GFP signal intensities at the
928 SPBs of cells with metaphase spindles (spindle length = 1,5-2 µm). Graph is plotted as
929 described in B. **D.** Analysis of Bfa1-GFP signal intensities at the SPBs of *kar9*Δ, *kar9*Δ *kin4*Δ
930 and *kar9*Δ *bud14*Δ cells with correctly aligned and misaligned anaphase spindles. The graph
931 was plotted as in B. Pairwise comparisons were performed using One-way Anova with
932 uncorrected Fisher's LSD *** $p < 0.001$, **** $p < 0.0001$, n: sample size. Scale bar: 2 µm.

933 **Figure 6- Figure Supplement 2. Analysis of Mob1 SPB localization. A.** Percentage of
934 metaphase cells (spindle length = 1,5-2 µm) with Mob1-GFP signal at the SPBs of the indicated
935 cells. Graphs are average of three independent experiments. A minimum of 100 cells were
936 counted from each strain in each experiment. Error bars show standard deviation. **B.**

937 Representative still images showing Mob1-GFP localization in metaphase cells **C-D.** Dot plot
938 of Mob1-GFP signal intensity at the SPBs of indicated strains carrying *MOB1-GFP mCherry-*
939 *TUB1* in metaphase (C) and anaphase (D). Black lines represent the mean value, and grey lines
940 show standard deviation. **E.** Representative still images of anaphase cells. Scale bar: 2 µm.
941 One-way Anova with uncorrected Fisher's LSD was used for pairwise comparisons. **** $p <$
942 0.0001.

943 **Figure 6 – Figure Supplement 3. Bfa1-GFP localization during spindle misalignment.**
944 Selected frames from time-lapse series of *BFA1-GFP SPC42-eqFP mCherry-TUB1* bearing
945 *kar9*Δ (A), *kar9*Δ *bud14*Δ (B) and *kar9*Δ *kin4*Δ (C) gene deletions. Cell boundaries are outlined
946 with a dashed line. Blue arrows indicate the SPBs. Time points from the beginning of the time
947 lapse is indicated on the frames. Scale bar: 2 µm.

948 **Figure 7 – Figure Supplement 1. Analysis of Bfa1 mobility in *lte1*Δ and *lte1*Δ *kin4*Δ cells.**
949 **A.** Bfa1-3HA Gal1-UPL-Tem1 containing *lte1*Δ and *lte1*Δ*kin4*Δ cells grown in galactose
950 containing medium were released from G1 arrest (t=0) into an alpha factor free medium
951 supplemented with glucose. Samples were collected at indicated time points. Bfa1-3HA
952 mobility shift was analyzed via western blotting. **B.** Indicated time points of each cell type
953 from the experiment shown in A were loaded side-by-side for better comparison of Bfa1-3HA
954 mobility. **C.** Percentage of cells with single nucleus (1 DAPI) and two separate nuclei (2 DAPI)
955 as well as budding index of the experiment shown in A were plotted as a marker for cell cycle
956 progression.

957 **Figure 7 – Figure Supplement 2. Kin4 overexpression toxicity in *bud14*Δ cells and**
958 **phosphatase assay using Bud14-TAP. A.** Serial dilutions of indicated strains were spotted
959 on Glucose containing (YPD) and Galactose containing (YP Raf/Gal) agar plates. Gal1-
960 Bud14 overexpression is induced on Galactose containing plates. **B.** In vitro phosphatase

961 assay of immunoprecipitated Bud14-TAP. Bud14-TAP was pulled on IgG Sepharose beads
962 from the lysates of *BUD14-TAP GLC7-9myc* cells. Beads were incubated with Bfa1-3HA
963 purified from *BFA1-3HA Gal1-UPL-TEM1 kin4*Δ cells in the presence or absence of Okadaic
964 acid. Beads incubated with ESM356-1 cell lysates were used as a negative control. Bud14-
965 TAP levels were detected using anti-TAP, Glc7-9myc levels were detected using anti-myc,
966 and Bfa1-3HA was detected using anti-HA antibodies. Quantification of relative levels of
967 hypersphosphorylated Bfa1 is shown on the right. Each color represents a different
968 independent experiment. One-way Anova with uncorrected Fisher's LSD was applied for
969 statistical analysis. ** $p<0.01$.

970

971

972

973 **Tables**

974 **Table 1. Yeast strains used in this study.**

Strain Name	Description	Reference
AKY038	*ESM356 Bfa1-GFP-kanMX6 Spc42-eqFP-hphNT1 mCherry-Tub1-URA3*	This study
AKY043	*ESM356 BFA1-GFP-kanMX6 Spc42-eqFP-hphNT1 kar9Δ::klTRP1 pRS316-KAR9*	(Caydasi & Pereira, 2009)
AKY1533	*ESM356 leu2::LEU2-pGal1-KIN4*	This study
AKY1574	*ESM356 leu2::LEU2-pGal1-KIN4 bub2Δ::hphNT1*	This study
AKY2526	*FAY145 lte1Δ::kanMX6 pRS316-LTE1 spo12Δ::natNT2*	(Caydasi *et al.*, 2017)
AKY260	*ESM356 kar9Δ::HIS3MX6 pRS316-KAR9*	(Caydasi *et al.*, 2017)
AKY2916	*FAY145 lte1Δ::kanMX6 pRS316-LTE1 spo12Δ::natNT2 bud14Δ::HIS3MX6*	This study
AKY2917	*YPH499 GFP-Tub1-URA3 dyn1Δ::klTRP1 bud14Δ::HIS3MX6*	This study
AKY2918	*YPH499 GFP-Tub1-URA3 dyn1Δ::klTRP1 kin4Δ::hphNT1 bud14Δ::HIS3MX6*	This study
AKY315	*ESM356 kar9Δ::HIS3MX6 pRS316-KAR9 bfa1Δ::klTRP1*	(Caydasi *et al.*, 2017)
AKY321	*ESM356 kar9Δ::HIS3MX6 pRS316-KAR9 kin4Δ::klTRP1*	(Caydasi *et al.*, 2017)
AKY346	*YPH499 kar9Δ::klTRP1 pRS316-KAR9 GFP-Tub1-ADE2*	(Caydasi *et al.*, 2010b)
AKY351	*YPH499 kar9Δ::klTRP1 pRS316-KAR9 kin4Δ::HIS3MX6 GFP-Tub1-ADE2*	(Caydasi *et al.*, 2017)
AKY4001	*ESM356 leu2::LEU2-pGal1-KIN4 bud14Δ::klTRP1*	This study

AKY4006	*ESM356 KIN4-GFP-HIS3MX6 Spc42-eqFP-natNT2 bud14Δ::klTRP1 lte1Δ::hphNT1 mCherry-Tub1-URA3*	This study
AKY4007	*ESM356 Bub2-GFP-kanMX6 Spc42-eqFP-hphNT1 mCherry-Tub1-URA3*	This study
AKY4008	*ESM356 Tem1-GFP-kanMX6 Spc42-eqFP-hphNT1 bud14Δ::HIS3MX6 mCherry-Tub1-URA3*	This study
AKY4009	*ESM356 Bub2-GFP-kanMX6 Spc42-eqFP-hphNT1 bud14Δ::klTRP1 mCherry-Tub1-URA3*	This study
AKY4011	*ESM356 Bfa1-GFP-kanMX6 Spc42-eqFP-hphNT1 bud14Δ::klTRP1 mCherry-Tub1-URA3*	This study
AKY4012	*ESM356 Bfa1-GFP-kanMX6 Spc42-eqFP-hphNT1 mCherry-Tub1-URA3*	This study
AKY4013	*ESM356 Tem1-GFP-kanMX6 Spc42-eqFP-hphNT1 mCherry-Tub1-URA3*	This study
AKY4016	*ESM356 KIN4-GFP-HIS3MX6 Spc42-eqFP-natNT2 lte1Δ::URA3 mCherry-Tub1-klTRP1*	This study
AKY4028	*FAY145 lte1Δ::kanMX6 bud14Δ::HIS3MX6*	This study
AKY4036	*FAY145 lte1Δ::kanMX6 bud14Δ::HIS3MX6 pRS416-endogenous BUD14-promoter- GFP-BUD145A*	This study
AKY4038	*FAY145 lte1Δ::kanMX6 bud14Δ::HIS3MX6 pRS416-endogenous BUD14-promoter- GFP-BUD14ΔSH3*	This study
AKY404	*ESM356 KIN4-GFP-HIS3MX6 Spc42-eqFP-natNT2 rts1Δ::klTRP1*	(Caydasi *et al.*, 2010b)
AKY4040	*ESM356 Spc42-eqFP-hphNT1 BUD14-GFP-his3MX6 mCherry-Tub1-URA3*	This study

AKY4068	*YPH499 kar9Δ::klTRP1 pRS316-KAR9 GFP-Tub1-ADE2 bud14Δ::HIS3MX6 kin4Δ::hphNT1*	This study
AKY4078	*PAY704 MATa ade2-1 his3-11,15 leu2-3,112 ura3-1 can1-100 ssd1-d2 glc7::LEU2 trp1-1::GLC7::TRP1 kar9Δ::hphNT1*	This study
AKY4079	*PAY701 MATa ade2-1 his3-11,15 leu2-3,112 ura3-1 can1-100 ssd1-d2 glc7::LEU2 trp1-1::glc7-12::TRP1 kar9Δ::hphNT1*	This study
AKY4087	*ESM356 cdc15::CDC15-as1(L99G)-URA3 Bfa1-3HA- kITRP1 pGal1-Bud14-natNT2*	This study
AKY4088	*ESM356 Mob1-GFP-kanMX6 Spc42-eqFP-hphNT1 kin4Δ::natNT2 bud14Δ::HIS3MX6*	This study
AKY4091	*YPH499 cdc5-10 Bfa1-3HA-kITRP1 lte1Δ::natNT2 bud14Δ::HIS3MX6*	This study
AKY4094	*YPH499 cdc14-2 pRS316-CDC14 bfa1Δ::klTRP3*	This study
AKY4095	*YPH499 dbf2-2 pRS316-DBF2 bfa1Δ::klTRP3*	This study
AKY4102	*ESM356 Mob1-GFP-kanMX6 Spc42-eqFP-hphNT1 kin4Δ::natNT2 bud14Δ::HIS3MX6 mCherry-Tub1-LEU2*	This study
AKY415	*ESM356 KIN4-6HA-hphNT1 rts1Δ::klTRP1*	(Caydasi *et al.*, 2010b)
BKY032	*ESM356 BFA1-GFP-kanMX6 Spc42-eqFP-hphNT1 kar9Δ::klTRP1 pRS316-KAR9 kin4Δ::HIS3MX6*	(Caydasi & Pereira, 2009)
DGY001	*ESM356 KIN4-6HA-hphNT1 bud14Δ::klTRP1*	This study
DGY004	*ESM356 KIN4-GFP-HIS3MX6 Spc42-eqFP-natNT2 bud14Δ::klTRP1*	This study
DKY056	*YPH499 bud14Δ::kITRP3*	This study
DKY057	*YPH499 cdc14-2 pRS316-CDC14 bud14Δ::klTRP3*	This study

DKY058	*YPH499 mob1-67 pRS316-MOB1 bud14Δ::klTRP3*	This study
DKY060	*YPH499 dbf2-2 pRS316-DBF2 bud14Δ::klTRP3*	This study
DKY061	*YPH499 cdc15-1 pRS316-CDC15 bud14Δ::klTRP3*	This study
DKY063	*ESM356 KIN4-GFP-HIS3MX6 Spc42-eqFP611-natNT2 bud14Δ::klTRP1*	This study
DKY069	*FAY145 lte1Δ::kanMX6 pRS316-LTE1 bud14Δ::HIS3MX6*	This study
DKY070	*PAY704 MATa ade2-1 his3-11,15 leu2-3,112 ura3-1 can1-100 ssd1-d2 glc7::LEU2 trp1-1::GLC7::TRP1*	This study
DKY071	*PAY701 MATa ade2-1 his3-11,15 leu2-3,112 ura3-1 can1-100 ssd1-d2 glc7::LEU2 trp1-1::glc7-12::TRP1*	This study
DKY074	*PAY701 glc7::LEU2 trp1-1::glc7-12::TRP1 lte1Δ::HIS3MX6*	This study
DKY075	*PAY704 glc7::LEU2 trp1-1::GLC7::TRP1 lte1Δ::HIS3MX6*	This study
DKY078	*PAY704 glc7::LEU2 trp1-1::GLC7::TRP1 lte1Δ::HIS3MX6 pRS316-LTE1*	This study
DKY079	*PAY701 glc7::LEU2 trp1-1::glc7-12::TRP1 lte1Δ::HIS3MX6 pRS316-LTE1*	This study
DKY080	*PAY701 glc7::LEU2 trp1-1::glc7-12::TRP1 lte1Δ::HIS3MX6 pRS316-LTE1 spo12Δ::hphNT1*	This study
DKY081	*ESM356 BFA1-GFP-kanMX6 Spc42-eqFP hphNT1 kar9Δ::klTRP1 pRS316-KAR9 bud14Δ::HIS3MX6*	This study
DKY101	*ESM356 GAL1-UPL-TEM1::klTRP1 Bfa1-3HA-hphNT1*	This study
DKY113	*SGY37-VIII,3 bub2Δ::hphNT1*	This study

DKY115	*ESM356 Bfa1-3HA-hphNT1 kin4Δ::natNT2 pWS103 (pGal1-UPL-Tem1-kITRP1)*	This study
DKY118	*ESM356 GAL1-UPL-TEM1::kITRP1 Bfa1-3HA-hphNT1 lte1Δ::natNT2*	This study
DKY123	*YPH499 cdc5-10 Bfa1-3HA-hphNT1*	This study
DKY125	*ESM356 GAL1-UPL-TEM1::kITRP1 Bfa1-3HA-hphNT1 kin4Δ::natNT2 bud14Δ::HIS3MX6*	This study
DKY126	*ESM356 GAL1-UPL-TEM1::kITRP1 Bfa1-3HA-hphNT1 lte1Δ::natNT2 bud14Δ::HIS3MX6*	This study
DKY131	*FAY145 lte1Δ::kanMX6 pRS316-LTE1 bud14Δ::HIS3MX6 GFP BUD14 CEN URA*	This study
DKY132	*ESM356 bud14Δ::klTRP GFP BUD14 CEN URA*	This study
DKY135	*FAY145 lte1Δ::kanMX6 bud14Δ::HIS3MX6 pRS416-ADH-BUD14*	This study
DKY137	*FAY145 lte1Δ::kanMX6 bud14Δ::HIS3MX6 pRS416-ADH-BUD14-F379A*	This study
DKY145	*ESM356 kar9Δ::HIS3MX6 bud14Δ::klTRP1 pRS316*	This study
DKY147	*ESM356 kar9Δ::HIS3MX6 bud14Δ::klTRP1 pMK125*	This study
DKY149	*ESM356 kar9Δ::HIS3MX6 bud14Δ::klTRP1 pMK131*	This study
DKY167	*ESM356 KIN4-GFP-HIS3MX6 Spc42-eqFP-natNT2 bud14Δ::klTRP1 lte1Δ::hphNT1*	This study
DKY179	*YPH499 cdc5-10 pRS316-CDC5 bud14Δ::klTRP3*	This study
DKY188	*ESM356 KIN4-GFP-HIS3MX6 Spc42-eqFP-natNT2 lte1Δ::URA3*	This study
ESM2156	*YPH499 GFP-Tub1-URA3 dyn1Δ::klTRP1 kin4Δ::hphNT1*	(Pereira & Schiebel, 2005)

ESM2282	*YPH499 cdc15-1 pRS316-CDC15*	(Caydasi *et al.*, 2017)
ESM2283	*YPH499 dbf2-2 pRS316-DBF2*	(Caydasi *et al.*, 2017)
ESM2285	*YPH499 mob1-67 pRS316-MOB1*	(Caydasi *et al.*, 2017)
ESM2326	*ESM356 KIN4-6HA-hphNT1*	(Caydasi *et al.*, 2010b)
ESM356	*MATa ura3-52 leu2Δ1 his3Δ200 trp1Δ63*	(Pereira & Schiebel, 2001)
FAY145	*MATa ura3-52 his3Δ200 leu2Δ1 lte1Δ::kanMX6 pRS316-LTE1*	(Bertazzi *et al.*, 2011)
GPY1033	*ESM356-1 KIN4-GFP-his3MX6 Spc42-eqFP-natNT2*	(Pereira & Schiebel, 2005)
GPY1054	*ESM356 Mob1-GFP-kanMX6 Spc42-eqFP-hphNT1*	This study
GPY491	*YPH499 cdc14-2 pRS316- CDC14*	(Caydasi *et al.*, 2017)
GYBY005	*ESM356 Glc7-TAP-kanMX6 (CBP-Tev-4ProtA-kanMX6)*	This study
HKY099	*ESM356 BFA1-GFP-kanMX6 Spc42-eqFP-hphNT1 kar9Δ::klTRP1 pRS316-KAR9 mCherry-Tub1-LEU2*	This study
HKY100	*ESM356 BFA1-GFP-kanMX6 Spc42-eqFP-hphNT1 kar9Δ::klTRP1 pRS316-KAR9 kin4Δ::HIS3MX6 mCherry-Tub1-LEU2*	This study
HKY101	*ESM356 BFA1-GFP-kanMX6 Spc42-eqFP-hphNT1 kar9Δ::klTRP1 pRS316-KAR9 bud14Δ::HIS3MX6 mCherry-Tub1-LEU2*	This study
HKY114	*ESM356 Bfa1-GFP-kanMX6 Spc42-eqFP-hphNT1 mCherry-Tub1-LEU2 pRS416*	This study

HKY115	*ESM356 Bfa1-GFP-kanMX6 Spc42-eqFP-hphNT1 bud14Δ::klTRP1 mCherry-Tub1-LEU2 pRS416*	This study
HKY116	*ESM356 Bfa1-GFP-kanMX6 Spc42-eqFP-hphNT1 bud14Δ::klTRP1 mCherry-Tub1-LEU2 pRS416-BUD14*	This study
HKY133	*FAY145 lte1Δ::kanMX6 pRS316-LTE1 kel1Δ::hphNT1*	This study
HKY134	*FAY145 lte1Δ::kanMX6 pRS316-LTE1 kel2Δ::hphNT1*	This study
HKY135	*FAY145 lte1Δ::kanMX6 pRS316-LTE1 spo12Δ::natNT2 kel1Δ::hphNT1*	This study
HKY136	*FAY145 lte1Δ::kanMX6 pRS316-LTE1 spo12Δ::natNT2 kel2Δ::hphNT1*	This study
HKY139	*ESM356 kar9Δ::HIS3MX6 pRS316-KAR9 kel1Δ::hphNT1*	This study
HKY140	*ESM356 kar9Δ::HIS3MX6 pRS316-KAR9 kel2Δ::hphNT1*	This study
HKY155	*ESM356 BUD14-TAP-kanMX6*	This study
HKY164	*ESM356 Bud14-TAP-kanMX6 Glc7-9myc-HIS3MX6*	This study
HKY171	*ESM356 Mob1-GFP-kanMX6 Spc42-eqFP-hphNT1 mCherry-Tub1-LEU2*	This study
HKY172	*ESM356 Mob1-GFP-kanMX6 Spc42-eqFP-hphNT1 mCherry-Tub1-LEU2 bud14Δ::HIS3MX6*	This study
HKY173	*ESM356 Mob1-GFP-kanMX6 Spc42-eqFP-hphNT1 mCherry-Tub1-LEU2 kin4Δ::natNT2*	This study
HKY174	*ESM356 Mob1-GFP-kanMX6 Spc42-eqFP-hphNT1 mCherry-Tub1-LEU2 bfa1Δ::natNT2*	This study
HKY175	*YPH499 kar9Δ::klTRP1 pRS316-KAR9 GFP-Tub1-ADE2 bud14Δ::HIS3MX6 bfa1Δ::natNT2*	This study
HKY177	*YPH499 bfa1Δ::klTRP1*	This study

HKY180	*YPH499 mob1-67 pRS316-MOB1 bfa1Δ::klTRP3*	This study
HKY182	*YPH499 cdc15-1 pRS316-CDC15 bfa1Δ::klTRP3*	This study
HKY183	*YPH499 cdc5-10 pRS316-CDC5 bfa1Δ::klTRP3*	This study
HKY184	*ESM356 cdc15::CDC15-as1(L99G)-URA3 Bfa1-3HA- kITRP1 bud14Δ::HIS3MX6*	This study
HKY185	*ESM356 pRS416*	This study
HKY186	*ESM356 pMK60 (Bud14-GFP)*	This study
HKY187	*ESM356 pHK002 (Bud14-F379A-GFP)*	This study
HKY188	*ESM356 pDK003 (Bud14-ΔSH3-GFP)*	This study
HKY189	*ESM356 pDK001 (Bud14-5A-GFP)*	This study
HKY190	*ESM356 BFA1-GFP-kanMX6 Spc42-eqFP-hphNT1 bud14Δ::klTRP1 mCherry-TUB1-Leu2 pMK131*	This study
IKY075	*SGY37-VIII,3 kin4Δ::klTRP1*	This study
DKY133	*SGY37-VIII,3 bub2Δ::hphT1*	
IKY192	*ESM356 kar9Δ::HIS3MX6 bud14Δ::klTRP1 pRS416-endogenous BUD14-promoter- GFP-BUD14-5A*	This study
IKY193	*ESM356 kar9Δ::HIS3MX6 bud14Δ::klTRP1 pRS416-endogenous BUD14-promoter- GFP-BUD14-ΔSH3*	This study
JOY79	*YPH499 cdc5-10 pRS316-CDC5*	(Caydasi *et al.*, 2017)
PAY701	*W303 MATa ade2-1 his3-11,15 leu2-3,112 ura3-1 can1-100 ssd1-d2 glc7::LEU2 trp1-1::glc7-12::TRP1*	(Andrews & Stark, 2000)
PAY704	*W303 MATa ade2-1 his3-11,15 leu2-3,112 ura3-1 can1-100 ssd1-d2 glc7::LEU2 trp1-1::GLC7::TRP1*	(Andrews & Stark, 2000)

SEY032	*YPH499 kar9Δ::klTRP3 pRS316-KAR9 GFP-Tub1-ADE2 bud14Δ::HIS3MX6*	This study 975
SEY206	*ESM356 cdc15::CDC15-as1(L99G)-URA3 Bfa1-3HA- kITRP1*	This study 976
SEY212	*ESM356 cdc15::CDC15-as1(L99G)-URA3 Bfa1-3HA- kITRP1 Bud14-9myc-HIS3MX6*	This study
SEY218	*ESM356 cdc15::CDC15-as1(L99G)-URA3 Bfa1-3HA- kITRP1 bud14Δ::HIS3MX6 leu2::LEU2- pGal1-Bud14-9myc-hphNT1*	This study
SEY219	*ESM356 cdc15::CDC15-as1(L99G)-URA3 Bfa1-3HA- kITRP1 bud14Δ::HIS3MX6 leu2::LEU2- pGal1-Bud14- F379A-9myc-hphNT1*	This study
SGY37-VIII,3	*MATa leu2 his3 trp1 ADE2 ura3-52::URA3-lexA-op-LacZ*	(Geissler *et al*, 1996)
SHM562	*YPH499 GFP-Tub1-URA3 dyn1Δ::klTRP1*	(Maekawa *et al.*, 2007)
YDA101	*ESM356 kar9Δ::HIS3MX6 bud14Δ::klTRP1*	(Caydasi *et al.*, 2017)
YPH499	*MATa ura3-52 lys2-801 ade2-101 trp1Δ63 his3Δ200 leu2Δ1*	(Sikorski & Hieter, 1989)

977 **Table 2. Plasmids used in this study**

Plasmid Name	Description	Reference
pRS316	*URA3-dependent CEN-based yeast-E. coli* shuffle plasmid. *AmpR.*	(Sikorski & Hieter, 1989)
pRS416	*URA3-dependent CEN-based yeast-E. coli* shuffle plasmid. *AmpR.*	(Geissler *et al.*, 1996)
pAFS125	*GFP-TUB1-URA3* containing integration plasmid.	(Straight *et al.*, 1997)
pSM1027	*GFP-TUB1-ADE2 containing integration plasmid.*	(Caydasi *et al.*, 2010b)
pAK010	*mCherry-TUB1-kıTRP1* containing integration plasmid.	(Khmelinskii *et al*, 2007)
pAK011	*mCherry-TUB1-URA3* containing integration plasmid.	(Khmelinskii *et al.*, 2007)
pBK067	*mCherry-TUB1-LEU2* containing integration plasmid.	(Caydasi *et al.*, 2014)
pWS103-1	*pRS304-Gal1-UPL-TEM1*	(Shou *et al.*, 1999)
pMM5	p423-Gal1-lexA-Myc	(Geissler *et al.*, 1996)
pMM6	p425-Gal1-Gal4-HA.	(Geissler *et al.*, 1996)
pCDV471	*pEG202 ADH1-LexA-DBD-GLC7*	(Lenssen *et al.*, 2005)
pEG202	*2µm ADH1-LexA-DBD-HIS3*	(Pereira *et al*, 1999)
pCL2-1	*pMM6-BUB2*	(Hofken & Schiebel, 2004)
pCL4a-3	*pMM6-BFA1*	(Hofken & Schiebel, 2004)
pHA132-2	*pMM6-KIN4* (1-750 aa)	Gift from G. Pereira
pHA69-1	*pMM5-BUD14*	Gift from G. Pereira
pHA70-1	*pMM6-BUD14*	Gift from G. Pereira
pTH221	*pMM6-KEL*	(Hofken & Schiebel, 2004)
IKY006	*pMM5-BUD14-5A*	This Study
IKY007	*pMM5-BUD14-F379A*	This Study
IKY008	*pMM5-BUD14-ΔSH3*	This Study
IKY010	*pMM6-BUD14-5A*	This Study

IKY011	*pMM6-BUD14-F379A*	This Study
IKY012	*pMM6-BUD14-ΔSH3*	This Study
pMK125	*pRS416 ADH-BUD14*	(Knaus *et al.*, 2005)
pMK131	*pRS416 ADH-BUD14-F379A*	(Knaus *et al.*, 2005)
pMK60	*pRS416-endogenous BUD14-promoter-GFP-BUD14*	(Knaus *et al.*, 2005)
pDKY001	*pRS416-endogenous BUD14-promoter-GFP-BUD14*$^{5A\ (135A\ 137A\ 138A\ 139A\ 140A)}$	This Study
pDKY003	*pRS416-endogenous BUD14-promoter-GFP-BUD14*$^{\Delta SH3(\Delta aa\ 262–318)}$	This Study
pHK002	*pRS416-endogenous BUD14-promoter-GFP-Bud14-F379A*	This study
pGW399-1	*pRS316-KAR9*	(Caydasi *et al.*, 2010b)
pSM805	*pRS305-pGal1*	(Konig *et al*, 2010)
pHK003	*pSM805 pGal1-Bud14-Leu2*	This study
pHK004	*pSM805 pGal1-Bud14-F379A-Leu2*	This study
pIK007	*pMM5-Bud14-F379A*	This study
pSM903-4	*pRS316-LTE1*	(Hofken & Schiebel, 2002)
pSM908	*pRS316-DBF2*	(Caydasi *et al.*, 2017)
pSM926	*pRS316-MOB1*	(Caydasi *et al.*, 2017)
pUG120	*pRS316-CDC14*	(Gruneberg *et al.*, 2000)
pBS9	*pRS316-CDC15*	(Caydasi *et al.*, 2017)
pCL33	*pRS316-CDC5*	(Hofken & Schiebel, 2004)

978

979 **References**

980 Adames NR, Cooper JA (2000) Microtubule interactions with the cell cortex causing
981 nuclear movements in Saccharomyces cerevisiae. *J Cell Biol* 149: 863-874

982 Adames NR, Oberle JR, Cooper JA (2001) The surveillance mechanism of the spindle
983 position checkpoint in yeast. *J Cell Biol* 153: 159-168

984 Andrews PD, Stark MJ (2000) Type 1 protein phosphatase is required for maintenance
985 of cell wall integrity, morphogenesis and cell cycle progression in Saccharomyces cerevisiae.
986 *Journal of cell science* 113 (Pt 3): 507-520

987 Asakawa K, Yoshida S, Otake F, Toh-e A (2001) A novel functional domain of Cdc15
988 kinase is required for its interaction with Tem1 GTPase in Saccharomyces cerevisiae. *Genetics*
989 157: 1437-1450

990 Bardin AJ, Visintin R, Amon A (2000) A mechanism for coupling exit from mitosis to
991 partitioning of the nucleus. *Cell* 102: 21-31

992 Baro B, Queralt E, Monje-Casas F (2017) Regulation of Mitotic Exit in Saccharomyces
993 cerevisiae. *Methods in molecular biology* 1505: 3-17

994 Baro B, Rodriguez-Rodriguez JA, Calabria I, Hernaez ML, Gil C, Queralt E (2013) Dual
995 Regulation of the mitotic exit network (MEN) by PP2A-Cdc55 phosphatase. *PLoS genetics* 9:
996 e1003966

997 Beach DL, Thibodeaux J, Maddox P, Yeh E, Bloom K (2000) The role of the proteins
998 Kar9 and Myo2 in orienting the mitotic spindle of budding yeast. *Curr Biol* 10: 1497-1506

999 Bertazzi DT, Kurtulmus B, Pereira G (2011) The cortical protein Lte1 promotes mitotic
1000 exit by inhibiting the spindle position checkpoint kinase Kin4. *J Cell Biol* 193: 1033-1048

1001 Bialojan C, Takai A (1988) Inhibitory effect of a marine-sponge toxin, okadaic acid, on
1002 protein phosphatases. Specificity and kinetics. *Biochem J* 256: 283-290

1003 Bishop AC, Ubersax JA, Petsch DT, Matheos DP, Gray NS, Blethrow J, Shimizu E,
1004 Tsien JZ, Schultz PG, Rose MD *et al* (2000) A chemical switch for inhibitor-sensitive alleles
1005 of any protein kinase. *Nature* 407: 395-401

1006 Bloecher A, Venturi GM, Tatchell K (2000) Anaphase spindle position is monitored by
1007 the BUB2 checkpoint. *Nat Cell Biol* 2: 556-558

1008 Campbell IW, Zhou X, Amon A (2020) Spindle pole bodies function as signal amplifiers
1009 in the Mitotic Exit Network. *Molecular biology of the cell* 31: 906-916

1010 Caydasi AK, Ibrahim B, Pereira G (2010a) Monitoring spindle orientation: Spindle
1011 position checkpoint in charge. *Cell division* 5: 28

1012 Caydasi AK, Khmelinskii A, Duenas-Sanchez R, Kurtulmus B, Knop M, Pereira G
1013 (2017) Temporal and compartment-specific signals coordinate mitotic exit with spindle
1014 position. *Nature communications* 8: 14129

1015 Caydasi AK, Kurtulmus B, Orrico MI, Hofmann A, Ibrahim B, Pereira G (2010b) Elm1
1016 kinase activates the spindle position checkpoint kinase Kin4. *J Cell Biol* 190: 975-989

1017 Caydasi AK, Lohel M, Grunert G, Dittrich P, Pereira G, Ibrahim B (2012) A dynamical
1018 model of the spindle position checkpoint. *Molecular systems biology* 8: 582

1019 Caydasi AK, Micoogullari Y, Kurtulmus B, Palani S, Pereira G (2014) The 14-3-3
1020 protein Bmh1 functions in the spindle position checkpoint by breaking Bfa1 asymmetry at
1021 yeast centrosomes. *Molecular biology of the cell* 25: 2143-2151

1022 Caydasi AK, Pereira G (2009) Spindle alignment regulates the dynamic association of
1023 checkpoint proteins with yeast spindle pole bodies. *Dev Cell* 16: 146-156

1024 Caydasi AK, Pereira G (2012) SPOC alert--when chromosomes get the wrong direction.
1025 *Experimental cell research* 318: 1421-1427

1026 Caydasi AK, Pereira G (2017) Evaluation of the Dynamicity of Mitotic Exit Network
1027 and Spindle Position Checkpoint Components on Spindle Pole Bodies by Fluorescence
1028 Recovery After Photobleaching (FRAP). *Methods in molecular biology* 1505: 167-182

1029 Cenamor R, Jimenez J, Cid VJ, Nombela C, Sanchez M (1999) The budding yeast Cdc15
1030 localizes to the spindle pole body in a cell-cycle-dependent manner. *Mol Cell Biol Res Commun*
1031 2: 178-184

1032 Cheng J, Turkel N, Hemati N, Fuller MT, Hunt AJ, Yamashita YM (2008) Centrosome
1033 misorientation reduces stem cell division during ageing. *Nature* 456: 599-604

1034 Cheng YL, Chen RH (2010) The AAA-ATPase Cdc48 and cofactor Shp1 promote
1035 chromosome bi-orientation by balancing Aurora B activity. *Journal of cell science* 123: 2025-
1036 2034

1037 Chesarone M, Gould CJ, Moseley JB, Goode BL (2009) Displacement of formins from
1038 growing barbed ends by bud14 is critical for actin cable architecture and function. *Dev Cell* 16:
1039 292-302

1040 Cohen P, Klumpp S, Schelling DL (1989a) An improved procedure for identifying and
1041 quantitating protein phosphatases in mammalian tissues. *FEBS Lett* 250: 596-600

1042 Cohen P, Schelling DL, Stark MJ (1989b) Remarkable similarities between yeast and
1043 mammalian protein phosphatases. *FEBS Lett* 250: 601-606

1044 Cullen PJ, Sprague GF, Jr. (2002) The Glc7p-interacting protein Bud14p attenuates
1045 polarized growth, pheromone response, and filamentous growth in Saccharomyces cerevisiae.
1046 *Eukaryot Cell* 1: 884-894

1047 D'Aquino KE, Monje-Casas F, Paulson J, Reiser V, Charles GM, Lai L, Shokat KM,
1048 Amon A (2005) The protein kinase Kin4 inhibits exit from mitosis in response to spindle
1049 position defects. *Mol Cell* 19: 223-234

1050 Eshel D, Urrestarazu LA, Vissers S, Jauniaux JC, van Vliet-Reedijk JC, Planta RJ,
1051 Gibbons IR (1993) Cytoplasmic dynein is required for normal nuclear segregation in yeast.
1052 *Proc Natl Acad Sci U S A* 90: 11172-11176

1053 Eskin JA, Rankova A, Johnston AB, Alioto SL, Goode BL (2016) Common formin-
1054 regulating sequences in Smy1 and Bud14 are required for the control of actin cable assembly
1055 in vivo. *Molecular biology of the cell* 27: 828-837

1056 Falk JE, Campbell IW, Joyce K, Whalen J, Seshan A, Amon A (2016a) LTE1 promotes
1057 exit from mitosis by multiple mechanisms. *Molecular biology of the cell* 27: 3991-4001

1058 Falk JE, Chan LY, Amon A (2011) Lte1 promotes mitotic exit by controlling the
1059 localization of the spindle position checkpoint kinase Kin4. *Proc Natl Acad Sci U S A* 108:
1060 12584-12590

1061 Falk JE, Tsuchiya D, Verdaasdonk J, Lacefield S, Bloom K, Amon A (2016b) Spatial
1062 signals link exit from mitosis to spindle position. *eLife* 5

1063 Frenz LM, Lee SE, Fesquet D, Johnston LH (2000) The budding yeast Dbf2 protein
1064 kinase localises to the centrosome and moves to the bud neck in late mitosis. *Journal of cell*
1065 *science* 113 Pt 19: 3399-3408

1066 Gao K, Zhang Y, Shi Q, Zhang J, Zhang L, Sun H, Jiao D, Zhao X, Tao H, Wei Y *et al*
1067 (2018) iASPP-PP1 complex is required for cytokinetic abscission by controlling CEP55
1068 dephosphorylation. *Cell Death Dis* 9: 528

1069 Geissler S, Pereira G, Spang A, Knop M, Soues S, Kilmartin J, Schiebel E (1996) The
1070 spindle pole body component Spc98p interacts with the gamma-tubulin-like Tub4p of
1071 Saccharomyces cerevisiae at the sites of microtubule attachment. *The EMBO journal* 15: 3899-
1072 3911

1073 Geymonat M, Spanos A, Jensen S, Sedgwick SG (2010) Phosphorylation of Lte1 by Cdk
1074 prevents polarized growth during mitotic arrest in S. cerevisiae. *J Cell Biol* 191: 1097-1112

1075 Geymonat M, Spanos A, Smith SJ, Wheatley E, Rittinger K, Johnston LH, Sedgwick SG
1076 (2002) Control of mitotic exit in budding yeast. In vitro regulation of Tem1 GTPase by Bub2
1077 and Bfa1. *J Biol Chem* 277: 28439-28445

1078 Geymonat M, Spanos A, Walker PA, Johnston LH, Sedgwick SG (2003) In vitro
1079 regulation of budding yeast Bfa1/Bub2 GAP activity by Cdc5. *J Biol Chem* 278: 14591-14594

1080 Gould CJ, Chesarone-Cataldo M, Alioto SL, Salin B, Sagot I, Goode BL (2014)
1081 Saccharomyces cerevisiae Kelch proteins and Bud14 protein form a stable 520-kDa formin
1082 regulatory complex that controls actin cable assembly and cell morphogenesis. *J Biol Chem*
1083 289: 18290-18301

1084 Gruneberg U, Campbell K, Simpson C, Grindlay J, Schiebel E (2000) Nud1p links astral
1085 microtubule organization and the control of exit from mitosis. *The EMBO journal* 19: 6475-
1086 6488

1087 Hofken T, Schiebel E (2002) A role for cell polarity proteins in mitotic exit. *The EMBO*
1088 *journal* 21: 4851-4862

1089 Hofken T, Schiebel E (2004) Novel regulation of mitotic exit by the Cdc42 effectors Gic1
1090 and Gic2. *J Cell Biol* 164: 219-231

1091 Holder J, Poser E, Barr FA (2019) Getting out of mitosis: spatial and temporal control of
1092 mitotic exit and cytokinesis by PP1 and PP2A. *FEBS Lett* 593: 2908-2924

1093 Hu F, Wang Y, Liu D, Li Y, Qin J, Elledge SJ (2001) Regulation of the Bub2/Bfa1 GAP
1094 complex by Cdc5 and cell cycle checkpoints. *Cell* 107: 655-665

1095 Janke C, Magiera MM, Rathfelder N, Taxis C, Reber S, Maekawa H, Moreno-Borchart
1096 A, Doenges G, Schwob E, Schiebel E *et al* (2004) A versatile toolbox for PCR-based tagging
1097 of yeast genes: new fluorescent proteins, more markers and promoter substitution cassettes.
1098 *Yeast* 21: 947-962

1099 Jaspersen SL, Charles JF, Tinker-Kulberg RL, Morgan DO (1998) A late mitotic
1100 regulatory network controlling cyclin destruction in Saccharomyces cerevisiae. *Molecular*
1101 *biology of the cell* 9: 2803-2817

1102 Kelly AE, Funabiki H (2009) Correcting aberrant kinetochore microtubule attachments:
1103 an Aurora B-centric view. *Curr Opin Cell Biol* 21: 51-58

1104 Khmelinskii A, Lawrence C, Roostalu J, Schiebel E (2007) Cdc14-regulated midzone
1105 assembly controls anaphase B. *J Cell Biol* 177: 981-993

1106 Kim HS, Fernandes G, Lee CW (2016) Protein Phosphatases Involved in Regulating
1107 Mitosis: Facts and Hypotheses. *Mol Cells* 39: 654-662

1108 Kim J, Luo G, Bahk YY, Song K (2012) Cdc5-dependent asymmetric localization of
1109 bfa1 fine-tunes timely mitotic exit. *PLoS genetics* 8: e1002450

1110 Knaus M, Cameroni E, Pedruzzi I, Tatchell K, De Virgilio C, Peter M (2005) The
1111 Bud14p-Glc7p complex functions as a cortical regulator of dynein in budding yeast. *The*
1112 *EMBO journal* 24: 3000-3011

1113 Knop M, Siegers K, Pereira G, Zachariae W, Winsor B, Nasmyth K, Schiebel E (1999)
1114 Epitope tagging of yeast genes using a PCR-based strategy: more tags and improved practical
1115 routines. *Yeast* 15: 963-972

1116 Konig C, Maekawa H, Schiebel E (2010) Mutual regulation of cyclin-dependent kinase
1117 and the mitotic exit network. *J Cell Biol* 188: 351-368

1118 Kotwaliwale C, Biggins S (2006) Microtubule capture: a concerted effort. *Cell* 127:
1119 1105-1108

1120 Krogan NJ, Cagney G, Yu H, Zhong G, Guo X, Ignatchenko A, Li J, Pu S, Datta N,
1121 Tikuisis AP *et al* (2006) Global landscape of protein complexes in the yeast Saccharomyces
1122 cerevisiae. *Nature* 440: 637-643

1123 Lee SE, Frenz LM, Wells NJ, Johnson AL, Johnston LH (2001a) Order of function of
1124 the budding-yeast mitotic exit-network proteins Tem1, Cdc15, Mob1, Dbf2, and Cdc5. *Curr*
1125 *Biol* 11: 784-788

1126 Lee SE, Jensen S, Frenz LM, Johnson AL, Fesquet D, Johnston LH (2001b) The Bub2-
1127 dependent mitotic pathway in yeast acts every cell cycle and regulates cytokinesis. *Journal of*
1128 *cell science* 114: 2345-2354

1129 Lenssen E, James N, Pedruzzi I, Dubouloz F, Cameroni E, Bisig R, Maillet L, Werner
1130 M, Roosen J, Petrovic K *et al* (2005) The Ccr4-Not complex independently controls both
1131 Msn2-dependent transcriptional activation--via a newly identified Glc7/Bud14 type I protein
1132 phosphatase module--and TFIID promoter distribution. *Mol Cell Biol* 25: 488-498

1133 Li YY, Yeh E, Hays T, Bloom K (1993) Disruption of mitotic spindle orientation in a
1134 yeast dynein mutant. *Proc Natl Acad Sci U S A* 90: 10096-10100

1135 Luca FC, Mody M, Kurischko C, Roof DM, Giddings TH, Winey M (2001)
1136 Saccharomyces cerevisiae Mob1p is required for cytokinesis and mitotic exit. *Mol Cell Biol*
1137 21: 6972-6983

1138 Maekawa H, Priest C, Lechner J, Pereira G, Schiebel E (2007) The yeast centrosome
1139 translates the positional information of the anaphase spindle into a cell cycle signal. *J Cell Biol*
1140 179: 423-436

1141 Manzano-Lopez J, Monje-Casas F (2020) The Multiple Roles of the Cdc14 Phosphatase
1142 in Cell Cycle Control. *Int J Mol Sci* 21

1143 Meitinger F, Khmelinskii A, Morlot S, Kurtulmus B, Palani S, Andres-Pons A, Hub B,
1144 Knop M, Charvin G, Pereira G (2014) A memory system of negative polarity cues prevents
1145 replicative aging. *Cell* 159: 1056-1069

1146 Meitinger F, Palani S, Pereira G (2016) Detection of Phosphorylation Status of
1147 Cytokinetic Components. *Methods in molecular biology* 1369: 219-237

1148 Meraldi P, Nigg EA (2001) Centrosome cohesion is regulated by a balance of kinase and
1149 phosphatase activities. *Journal of cell science* 114: 3749-3757

1150 Miller RK, Rose MD (1998) Kar9p is a novel cortical protein required for cytoplasmic
1151 microtubule orientation in yeast. *J Cell Biol* 140: 377-390

1152 Molk JN, Schuyler SC, Liu JY, Evans JG, Salmon ED, Pellman D, Bloom K (2004) The
1153 differential roles of budding yeast Tem1p, Cdc15p, and Bub2p protein dynamics in mitotic
1154 exit. *Molecular biology of the cell* 15: 1519-1532

1155 Monje-Casas F, Amon A (2009) Cell polarity determinants establish asymmetry in MEN
1156 signaling. *Dev Cell* 16: 132-145

1157 Morishita T, Mitsuzawa H, Nakafuku M, Nakamura S, Hattori S, Anraku Y (1995)
1158 Requirement of Saccharomyces cerevisiae Ras for completion of mitosis. *Science* 270: 1213-
1159 1215

1160 Moura M, Conde C (2019) Phosphatases in Mitosis: Roles and Regulation. *Biomolecules*
1161 9

1162 Musacchio A, Salmon ED (2007) The spindle-assembly checkpoint in space and time.
1163 *Nature reviews Molecular cell biology* 8: 379-393

1164 Nasa I, Kettenbach AN (2018) Coordination of Protein Kinase and Phosphoprotein
1165 Phosphatase Activities in Mitosis. *Front Cell Dev Biol* 6: 30

1166 Neller J, Dunkler A, Rosler R, Johnsson N (2015) A protein complex containing Epo1p
1167 anchors the cortical endoplasmic reticulum to the yeast bud tip. *J Cell Biol* 208: 71-87

1168 O'Connell CB, Wang YL (2000) Mammalian spindle orientation and position respond to
1169 changes in cell shape in a dynein-dependent fashion. *Molecular biology of the cell* 11: 1765-
1170 1774

1171 Perdiguero E, Nebreda AR (2004) Regulation of Cdc25C activity during the meiotic
1172 G2/M transition. *Cell Cycle* 3: 733-737

1173 Pereira G, Grueneberg U, Knop M, Schiebel E (1999) Interaction of the yeast gamma-
1174 tubulin complex-binding protein Spc72p with Kar1p is essential for microtubule function
1175 during karyogamy. *The EMBO journal* 18: 4180-4195

1176 Pereira G, Hofken T, Grindlay J, Manson C, Schiebel E (2000) The Bub2p spindle
1177 checkpoint links nuclear migration with mitotic exit. *Mol Cell* 6: 1-10

1178 Pereira G, Manson C, Grindlay J, Schiebel E (2002) Regulation of the Bfa1p-Bub2p
1179 complex at spindle pole bodies by the cell cycle phosphatase Cdc14p. *J Cell Biol* 157: 367-379

1180 Pereira G, Schiebel E (2001) The role of the yeast spindle pole body and the mammalian
1181 centrosome in regulating late mitotic events. *Curr Opin Cell Biol* 13: 762-769

1182 Pereira G, Schiebel E (2005) Kin4 kinase delays mitotic exit in response to spindle
1183 alignment defects. *Mol Cell* 19: 209-221

1184 Pereira G, Yamashita YM (2011) Fly meets yeast: checking the correct orientation of cell
1185 division. *Trends Cell Biol*

1186 Pinsky BA, Kotwaliwale CV, Tatsutani SY, Breed CA, Biggins S (2006) Glc7/protein
1187 phosphatase 1 regulatory subunits can oppose the Ipl1/aurora protein kinase by redistributing
1188 Glc7. *Mol Cell Biol* 26: 2648-2660

1189 Rock JM, Amon A (2009) The FEAR network. *Curr Biol* 19: R1063-1068

1190 Ruchaud S, Carmena M, Earnshaw WC (2007) Chromosomal passengers: conducting
1191 cell division. *Nature reviews Molecular cell biology* 8: 798-812

1192 Scarfone I, Piatti S (2015) Coupling spindle position with mitotic exit in budding yeast:
1193 The multifaceted role of the small GTPase Tem1. *Small GTPases* 6: 196-201

1194 Scarfone I, Venturetti M, Hotz M, Lengefeld J, Barral Y, Piatti S (2015) Asymmetry of
1195 the budding yeast Tem1 GTPase at spindle poles is required for spindle positioning but not for
1196 mitotic exit. *PLoS genetics* 11: e1004938

1197 Seshan A, Bardin AJ, Amon A (2002) Control of Lte1 localization by cell polarity
1198 determinants and Cdc14. *Curr Biol* 12: 2098-2110

1199 Sherman F (1991) Getting started with yeast. *Methods Enzymol* 194: 3-21

1200 Shirayama M, Matsui Y, Tanaka K, Toh-e A (1994a) Isolation of a CDC25 family gene,
1201 MSI2/LTE1, as a multicopy suppressor of ira1. *Yeast* 10: 451-461

1202 Shirayama M, Matsui Y, Toh EA (1994b) The yeast TEM1 gene, which encodes a GTP-
1203 binding protein, is involved in termination of M phase. *Mol Cell Biol* 14: 7476-7482

1204 Shou W, Seol JH, Shevchenko A, Baskerville C, Moazed D, Chen ZW, Jang J,
1205 Charbonneau H, Deshaies RJ (1999) Exit from mitosis is triggered by Tem1-dependent release
1206 of the protein phosphatase Cdc14 from nucleolar RENT complex. *Cell* 97: 233-244

1207 Sikorski RS, Hieter P (1989) A system of shuttle vectors and yeast host strains designed
1208 for efficient manipulation of DNA in Saccharomyces cerevisiae. *Genetics* 122: 19-27

1209 Siller KH, Doe CQ (2009) Spindle orientation during asymmetric cell division. *Nat Cell*
1210 *Biol* 11: 365-374

1211 Stegmeier F, Visintin R, Amon A (2002) Separase, polo kinase, the kinetochore protein
1212 Slk19, and Spo12 function in a network that controls Cdc14 localization during early anaphase.
1213 *Cell* 108: 207-220

1214 Straight AF, Marshall WF, Sedat JW, Murray AW (1997) Mitosis in living budding
1215 yeast: anaphase A but no metaphase plate. *Science* 277: 574-578

1216 Valerio-Santiago M, Monje-Casas F (2011) Tem1 localization to the spindle pole bodies
1217 is essential for mitotic exit and impairs spindle checkpoint function. *J Cell Biol* 192: 599-614

1218 Visintin R, Amon A (2001) Regulation of the mitotic exit protein kinases Cdc15 and
1219 Dbf2. *Molecular biology of the cell* 12: 2961-2974

1220 Wang Y, Hu F, Elledge SJ (2000) The Bfa1/Bub2 GAP complex comprises a universal
1221 checkpoint required to prevent mitotic exit. *Curr Biol* 10: 1379-1382

1222 Weiss EL (2012) Mitotic Exit and Separation of Mother and Daughter Cells. *Genetics*
1223 192: 1165-1202

1224 Wu JQ, Guo JY, Tang W, Yang CS, Freel CD, Chen C, Nairn AC, Kornbluth S (2009)
1225 PP1-mediated dephosphorylation of phosphoproteins at mitotic exit is controlled by inhibitor-
1226 1 and PP1 phosphorylation. *Nat Cell Biol* 11: 644-651

1227 Yeh E, Skibbens RV, Cheng JW, Salmon ED, Bloom K (1995) Spindle dynamics and
1228 cell cycle regulation of dynein in the budding yeast, Saccharomyces cerevisiae. *J Cell Biol* 130:
1229 687-700

1230 Yoshida S, Toh-e A (2001) Regulation of the localization of Dbf2 and mob1 during cell
1231 division of saccharomyces cerevisiae. *Genes Genet Syst* 76: 141-147
1232

Figure 1

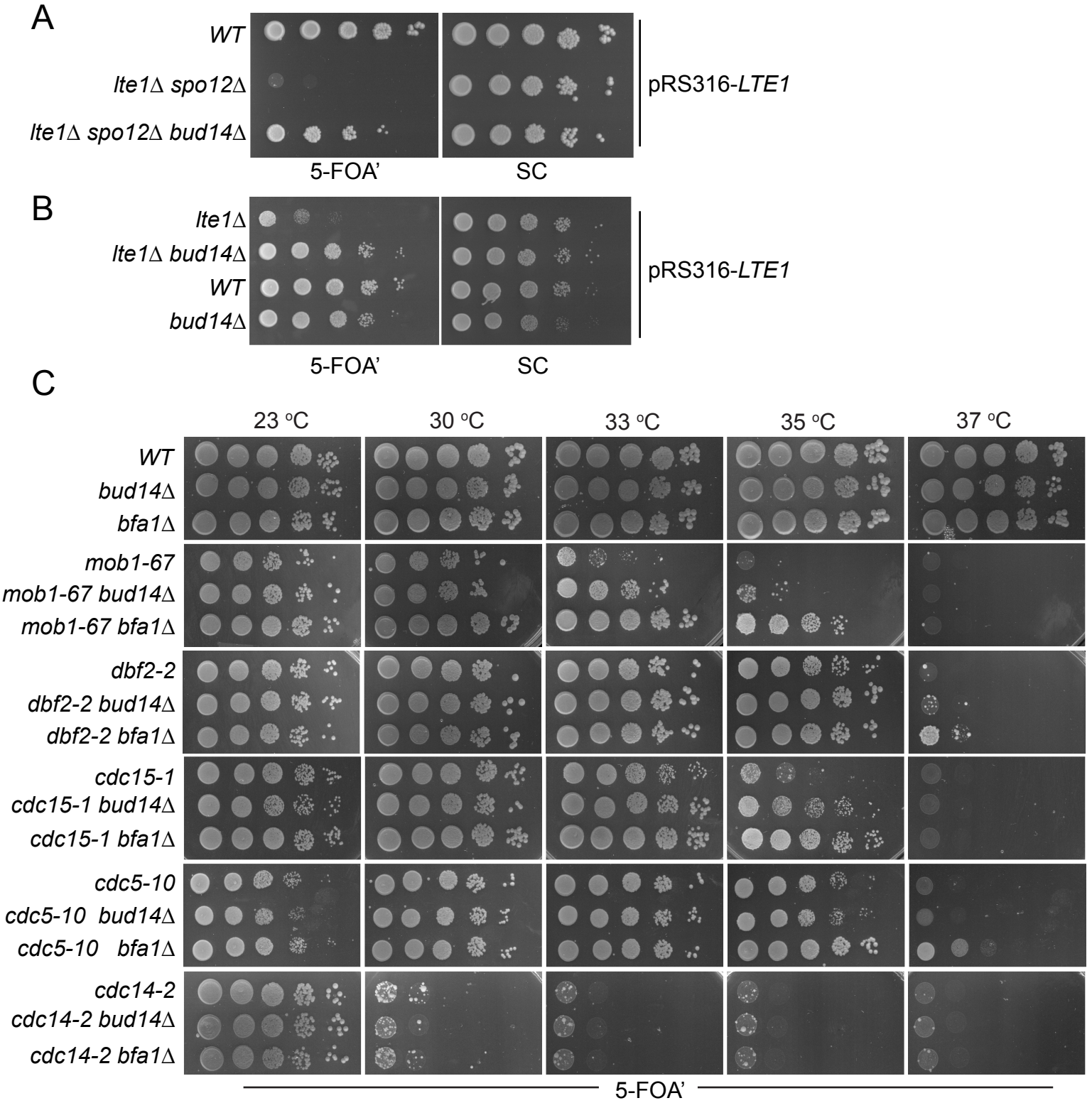
A
WT
lte1Δ spo12Δ
lte1Δ spo12Δ bud14Δ
pRS316-LTE1
5-FOA'
SC
B
lte1Δ
lte1Δ bud14Δ
WT
bud14Δ
pRS316-LTE1
5-FOA'
SC
C
23 °C
30 °C
33 °C
35 °C
37 °C
WT
bud14Δ
bfa1Δ
mob1-67
mob1-67 bud14Δ
mob1-67 bfa1Δ
dbf2-2
dbf2-2 bud14Δ
dbf2-2 bfa1Δ
cdc15-1
cdc15-1 bud14Δ
cdc15-1 bfa1Δ
cdc5-10
cdc5-10 bud14Δ
cdc5-10 bfa1Δ
cdc14-2
cdc14-2 bud14Δ
cdc14-2 bfa1Δ
5-FOA'

Figure 2

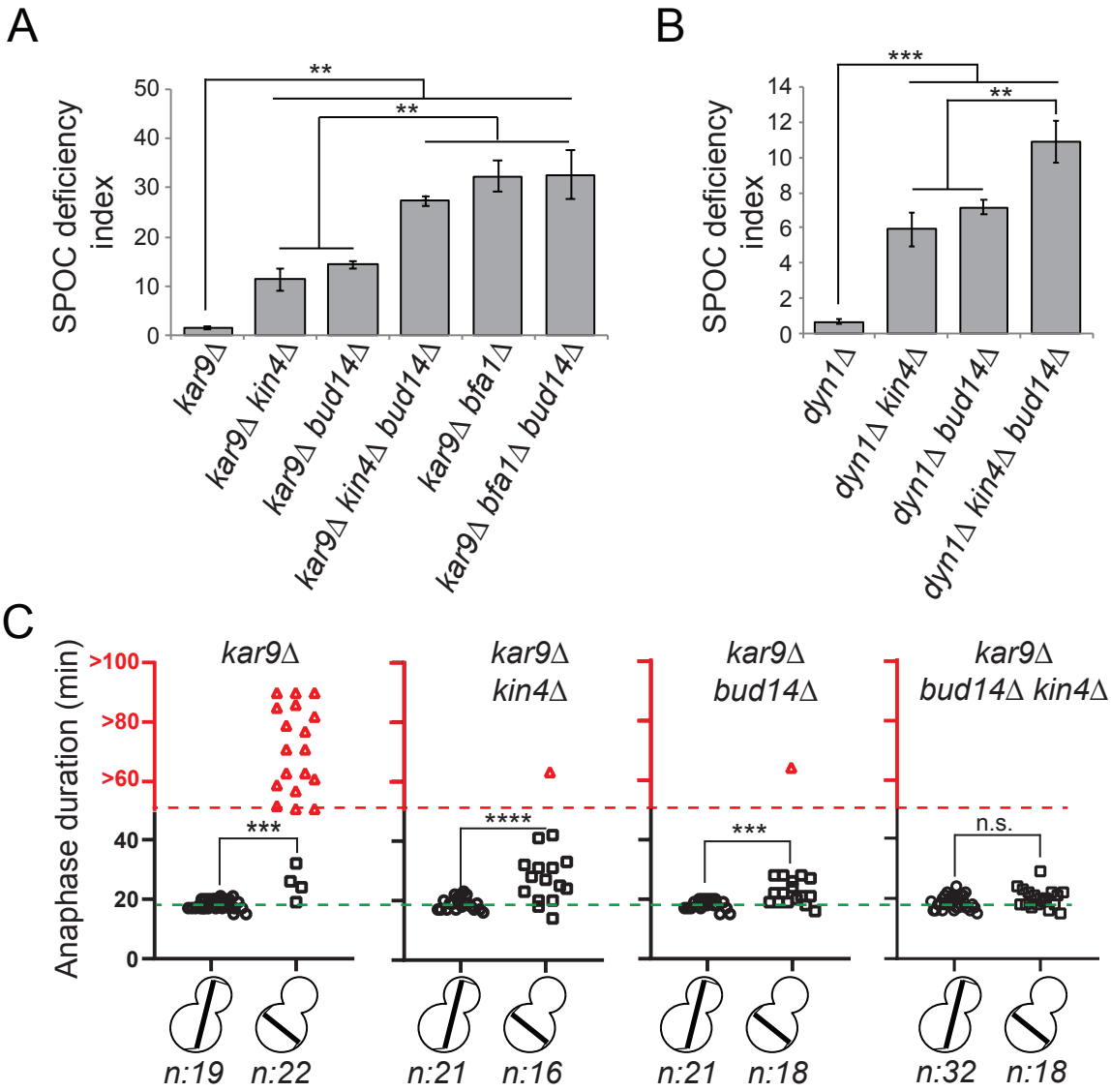
A
SPOC deficiency index
50
40
30
20
10
0
**
**
kar9Δ
kar9Δ kin4Δ
kar9Δ bud14Δ
kar9Δ kin4Δ bud14Δ
kar9Δ bfa1Δ
kar9Δ bfa1Δ bud14Δ
B
SPOC deficiency index
14
12
10
8
6
4
2
0
***
**
dyn1Δ
dyn1Δ kin4Δ
dyn1Δ bud14Δ
dyn1Δ kin4Δ bud14Δ
C
Anaphase duration (min)
>100
>80
>60
40
20
0
kar9Δ
kar9Δ kin4Δ
kar9Δ bud14Δ
kar9Δ bud14Δ kin4Δ
***
****
***
n.s.
n:19
n:22
n:21
n:16
n:21
n:18
n:32
n:18

Figure 3

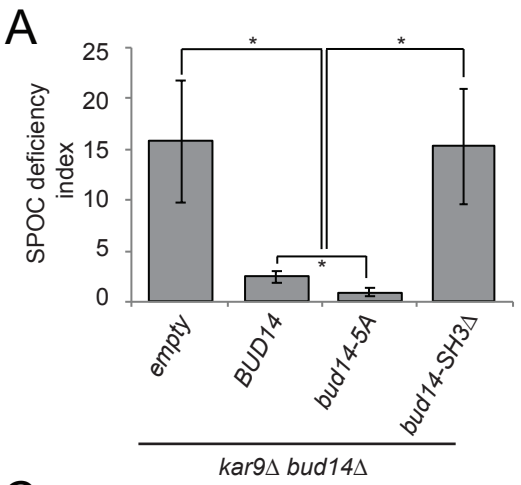
A
SPOC deficiency index
25
20
15
10
5
0
*
*
*
empty
BUD14
bud14-5A
bud14-SH3Δ
kar9Δ bud14Δ

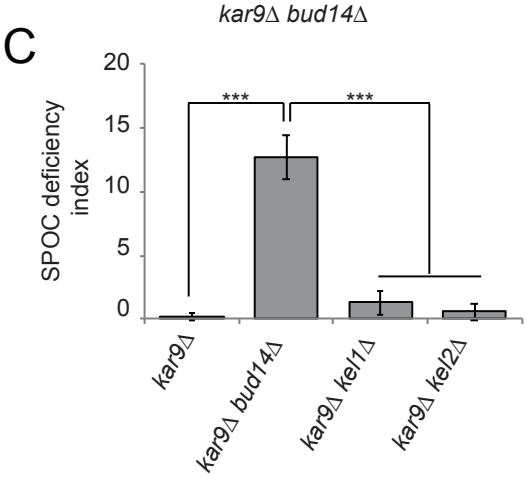
C
SPOC deficiency index
20
15
10
5
0
***
***
kar9Δ
kar9Δ bud14Δ
kar9Δ kel1Δ
kar9Δ kel2Δ

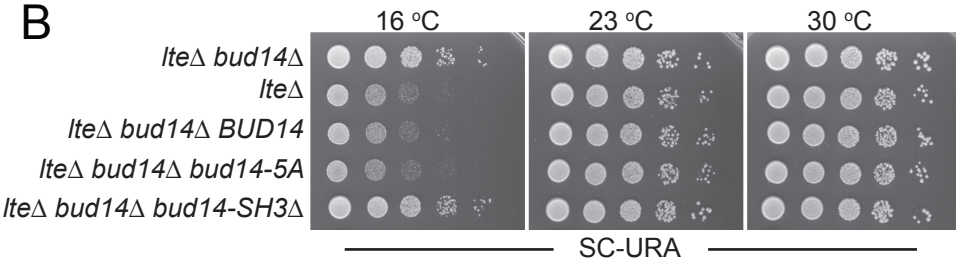
B
16 °C
23 °C
30 °C
lteΔ bud14Δ
lteΔ
lteΔ bud14Δ BUD14
lteΔ bud14Δ bud14-5A
lteΔ bud14Δ bud14-SH3Δ
SC-URA

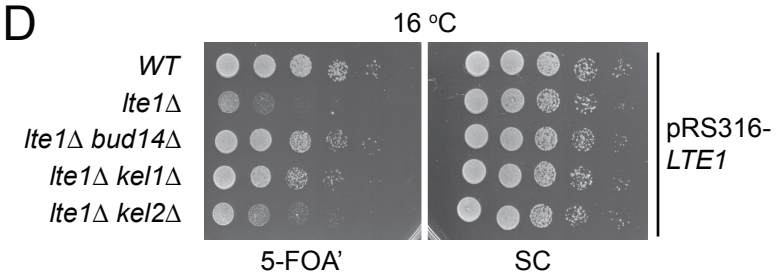
D
16 °C
WT
lte1Δ
lte1Δ bud14Δ
lte1Δ kel1Δ
lte1Δ kel2Δ
pRS316-LTE1
5-FOA'
SC

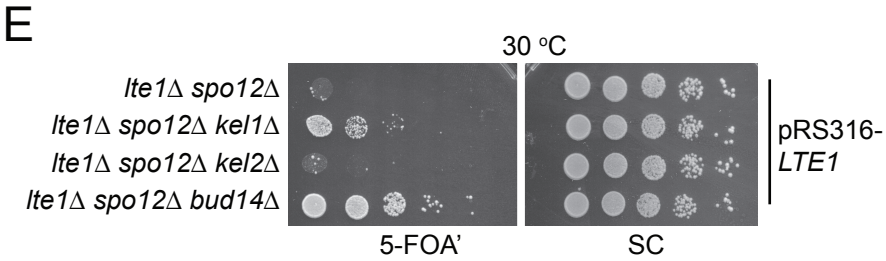
E
30 °C
lte1Δ spo12Δ
lte1Δ spo12Δ kel1Δ
lte1Δ spo12Δ kel2Δ
lte1Δ spo12Δ bud14Δ
pRS316-LTE1
5-FOA'
SC

Figure 4

A

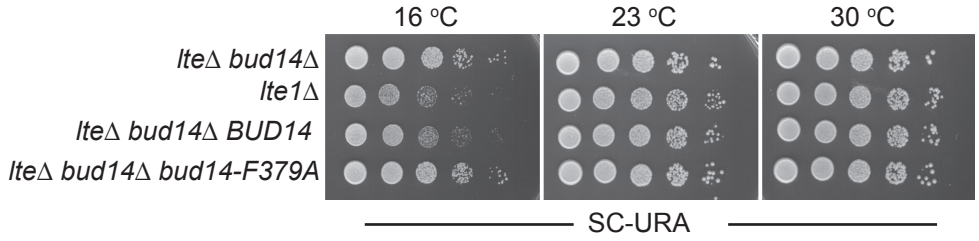

B

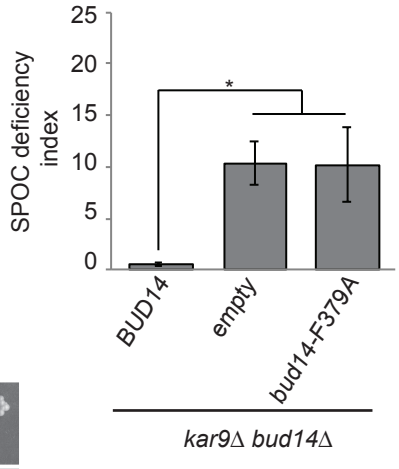

C

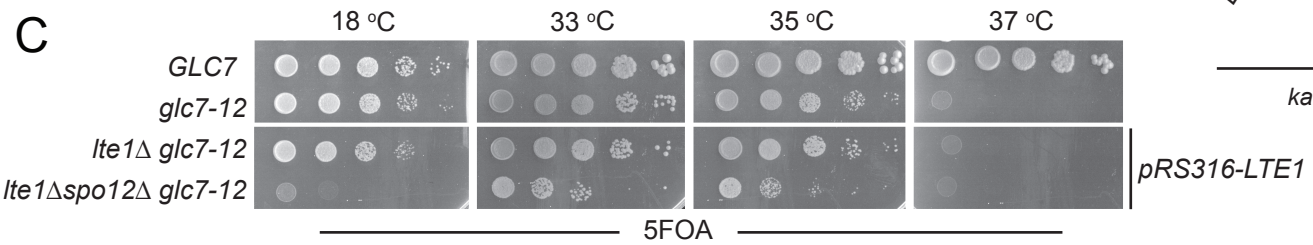

D

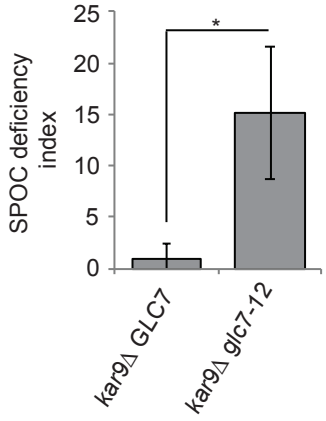

Figure 5

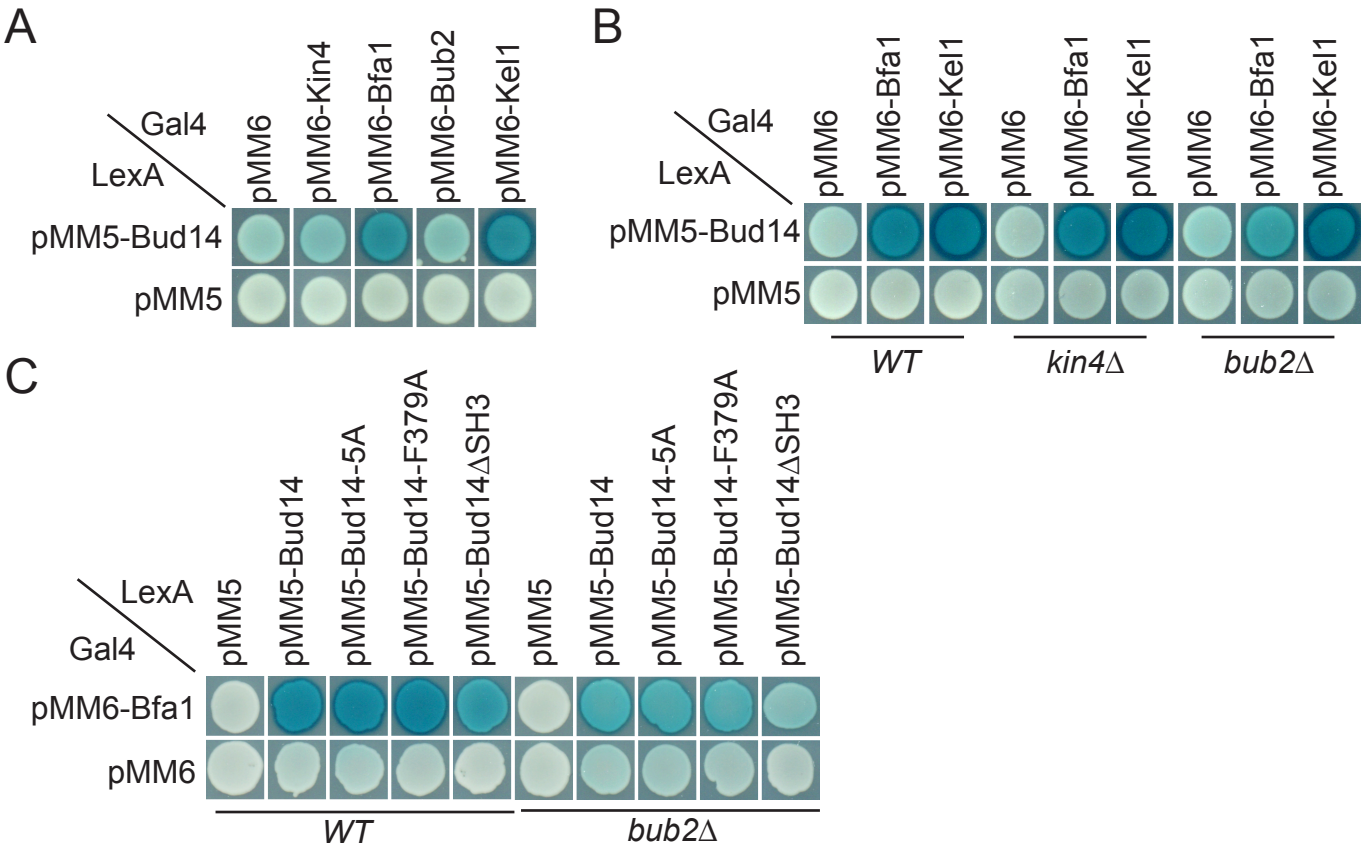
A
Gal4
LexA
pMM6
pMM6-Kin4
pMM6-Bfa1
pMM6-Bub2
pMM6-Kel1
pMM5-Bud14
pMM5
B
Gal4
LexA
pMM6
pMM6-Bfa1
pMM6-Kel1
pMM6
pMM6-Bfa1
pMM6-Kel1
pMM6
pMM6-Bfa1
pMM6-Kel1
pMM5-Bud14
pMM5
WT
kin4Δ
bub2Δ
C
LexA
Gal4
pMM5
pMM5-Bud14
pMM5-Bud14-5A
pMM5-Bud14-F379A
pMM5-Bud14ΔSH3
pMM5
pMM5-Bud14
pMM5-Bud14-5A
pMM5-Bud14-F379A
pMM5-Bud14ΔSH3
pMM6-Bfa1
pMM6
WT
bub2Δ

Figure 6

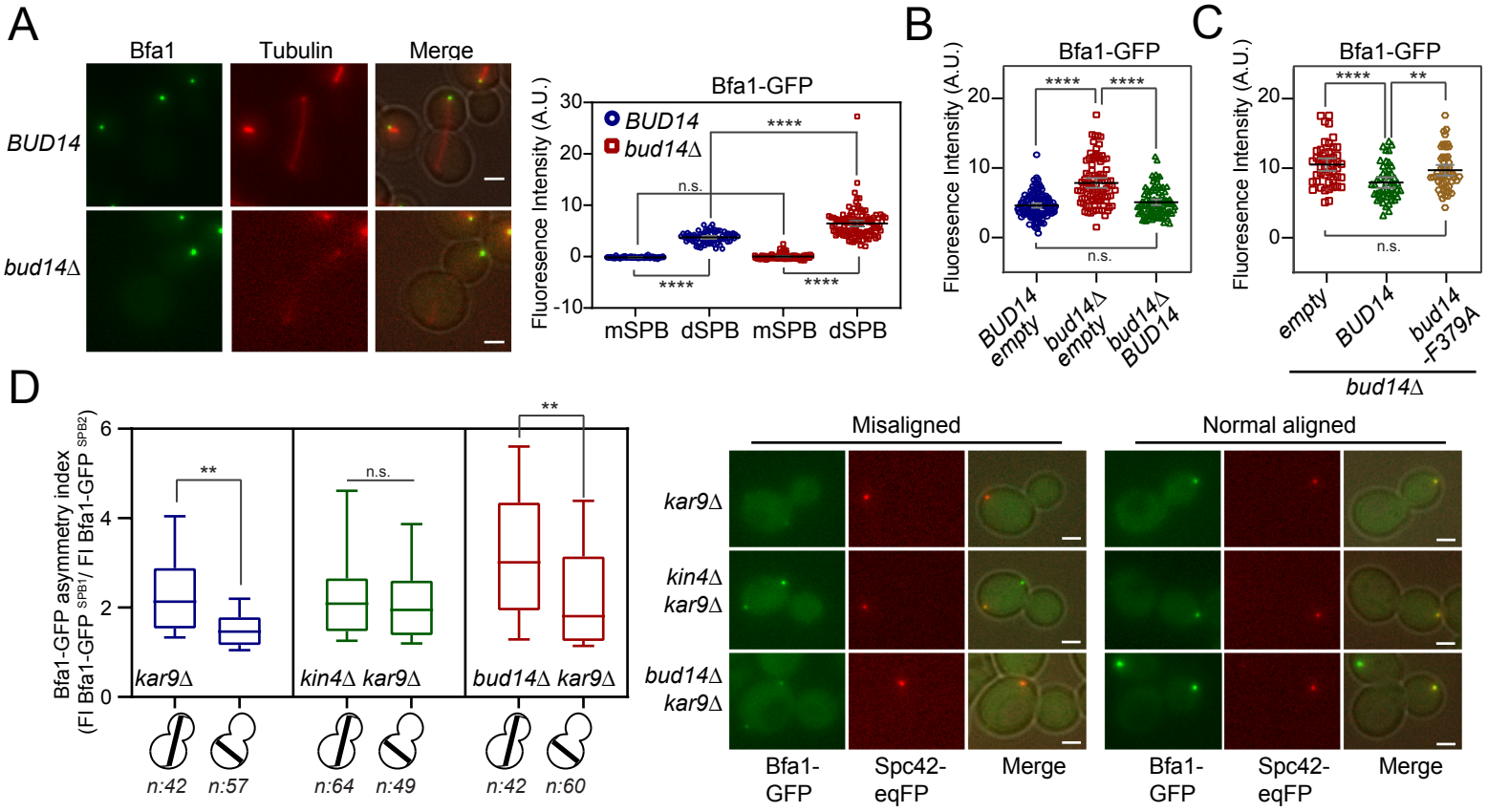
A
Bfa1
Tubulin
Merge
BUD14
bud14Δ
Bfa1-GFP
BUD14
bud14Δ
Fluoresence Intensity (A.U.)
30
20
10
0
-10
****
n.s.
****
****
mSPB
dSPB
mSPB
dSPB
B
Bfa1-GFP
Fluoresence Intensity (A.U.)
20
10
0
****
****
n.s.
BUD14 empty
bud14Δ empty
bud14Δ BUD14
C
Bfa1-GFP
Fluoresence Intensity (A.U.)
20
10
0
****
**
n.s.
empty
BUD14
bud14 -F379A
bud14Δ
D
Bfa1-GFP asymmetry index
(FI Bfa1-GFP SPB1/ FI Bfa1-GFP SPB2)
6
4
2
0
**
n.s.
**
kar9Δ
kin4Δ kar9Δ
bud14Δ kar9Δ
n:42
n:57
n:64
n:49
n:42
n:60
Misaligned
Normal aligned
kar9Δ
kin4Δ kar9Δ
bud14Δ kar9Δ
Bfa1-GFP
Spc42-eqFP
Merge
Bfa1-GFP
Spc42-eqFP
Merge

Figure 7

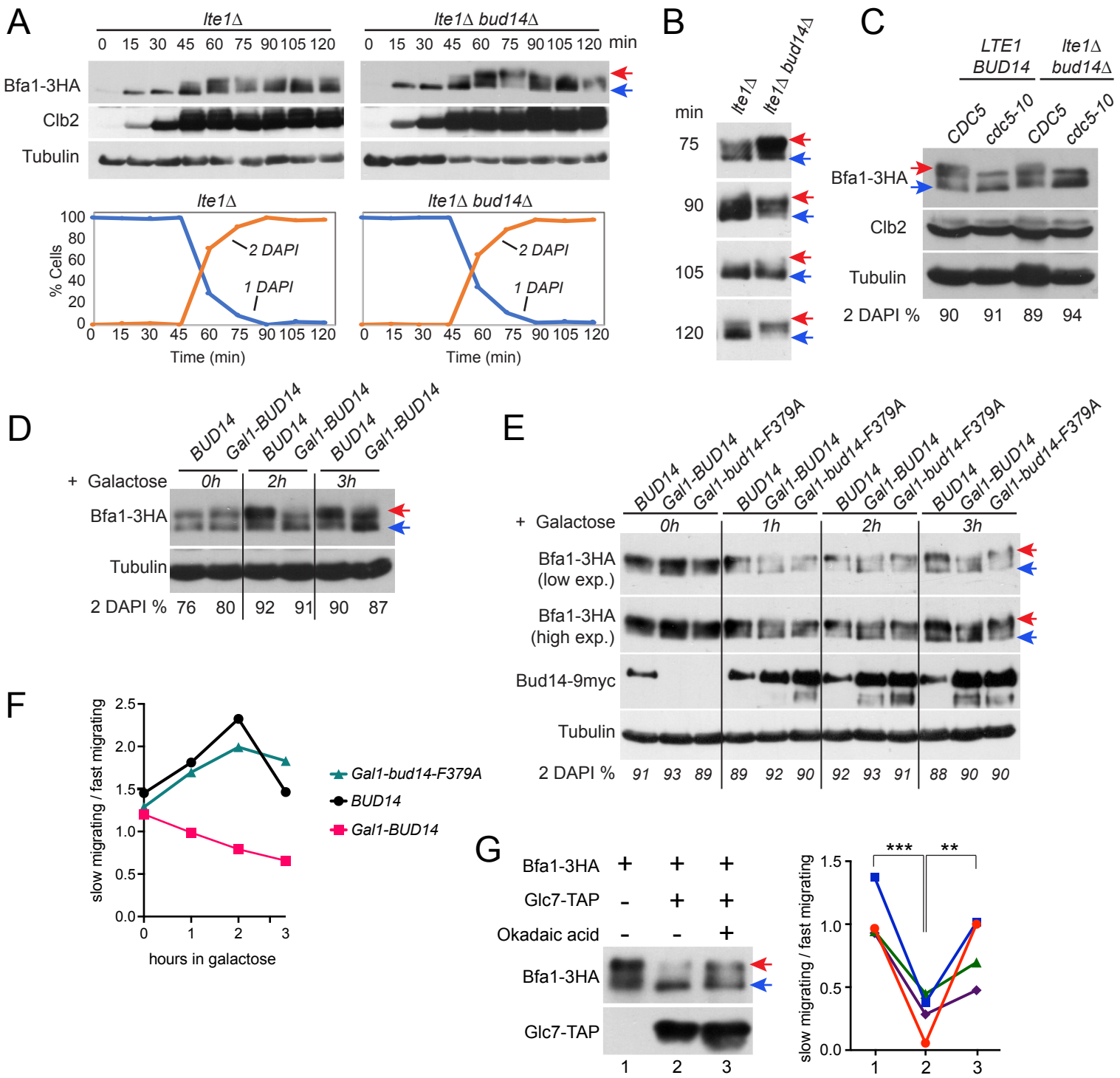
A
lte1Δ
lte1Δ bud14Δ
0 15 30 45 60 75 90 105 120 min
Bfa1-3HA
Clb2
Tubulin
% Cells
2 DAPI
1 DAPI
Time (min)
B
min
lte1Δ
lte1Δ bud14Δ
75
90
105
120
C
LTE1 BUD14
lte1Δ bud14Δ
CDC5
cdc5-10
Bfa1-3HA
Clb2
Tubulin
2 DAPI % 90 91 89 94
D
BUD14
Gal1-BUD14
+ Galactose
0h
2h
3h
Bfa1-3HA
Tubulin
2 DAPI % 76 80 92 91 90 87
E
Gal1-bud14-F379A
+ Galactose
0h
1h
2h
3h
Bfa1-3HA (low exp.)
Bfa1-3HA (high exp.)
Bud14-9myc
Tubulin
2 DAPI % 91 93 89 89 92 90 92 93 91 88 90 90
F
slow migrating / fast migrating
hours in galactose
Gal1-bud14-F379A
BUD14
Gal1-BUD14
G
Bfa1-3HA
Glc7-TAP
Okadaic acid
***
**

Figure 2 - Figure Supplement 1

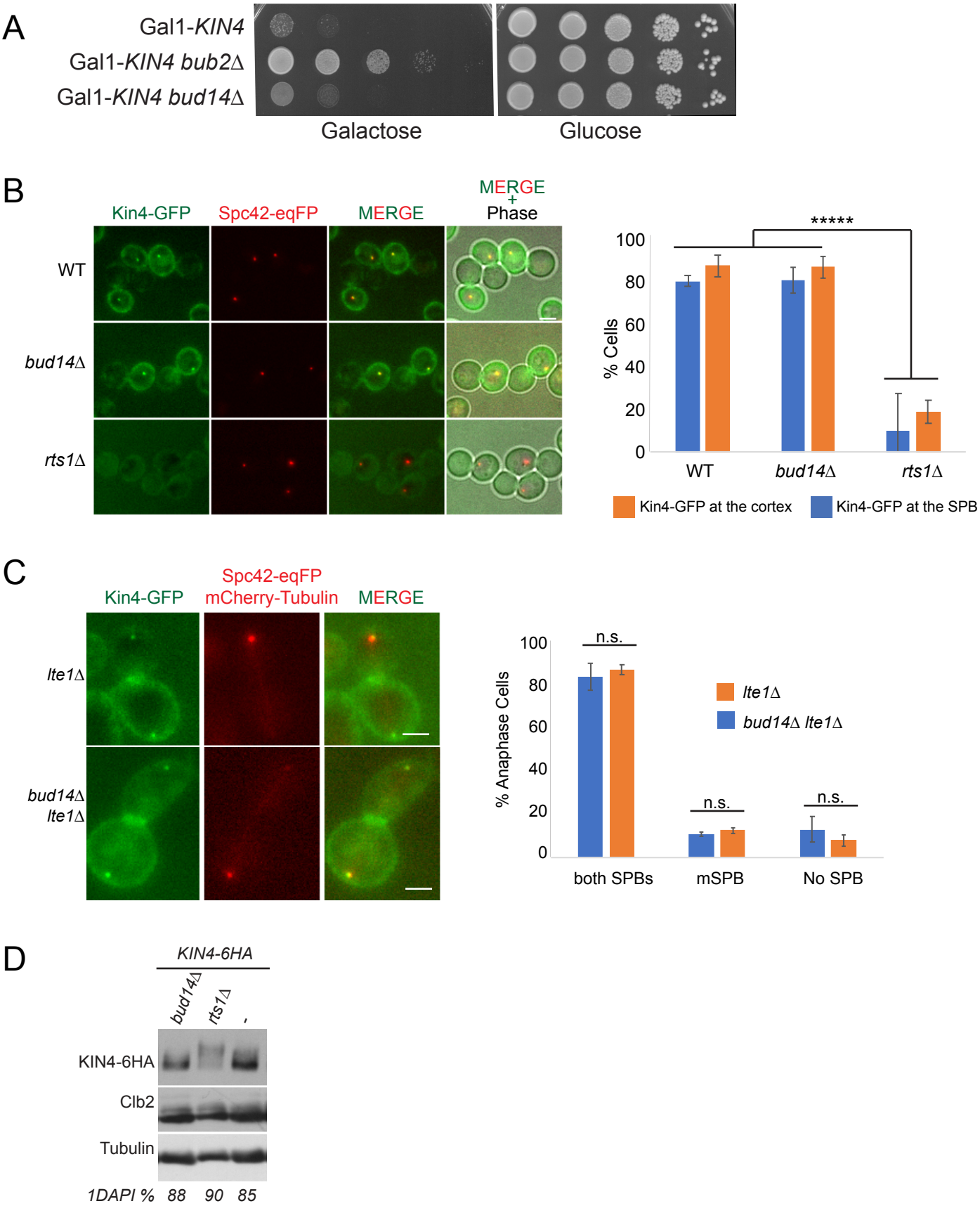

Figure 3 - Figure Supplement 1

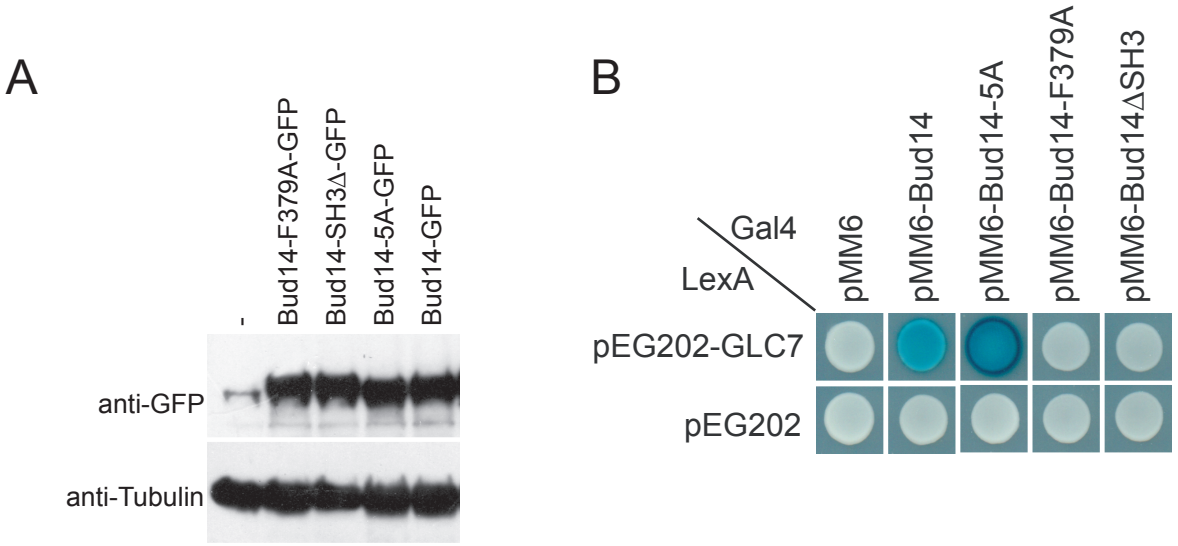

Figure 4 - Supplement 1

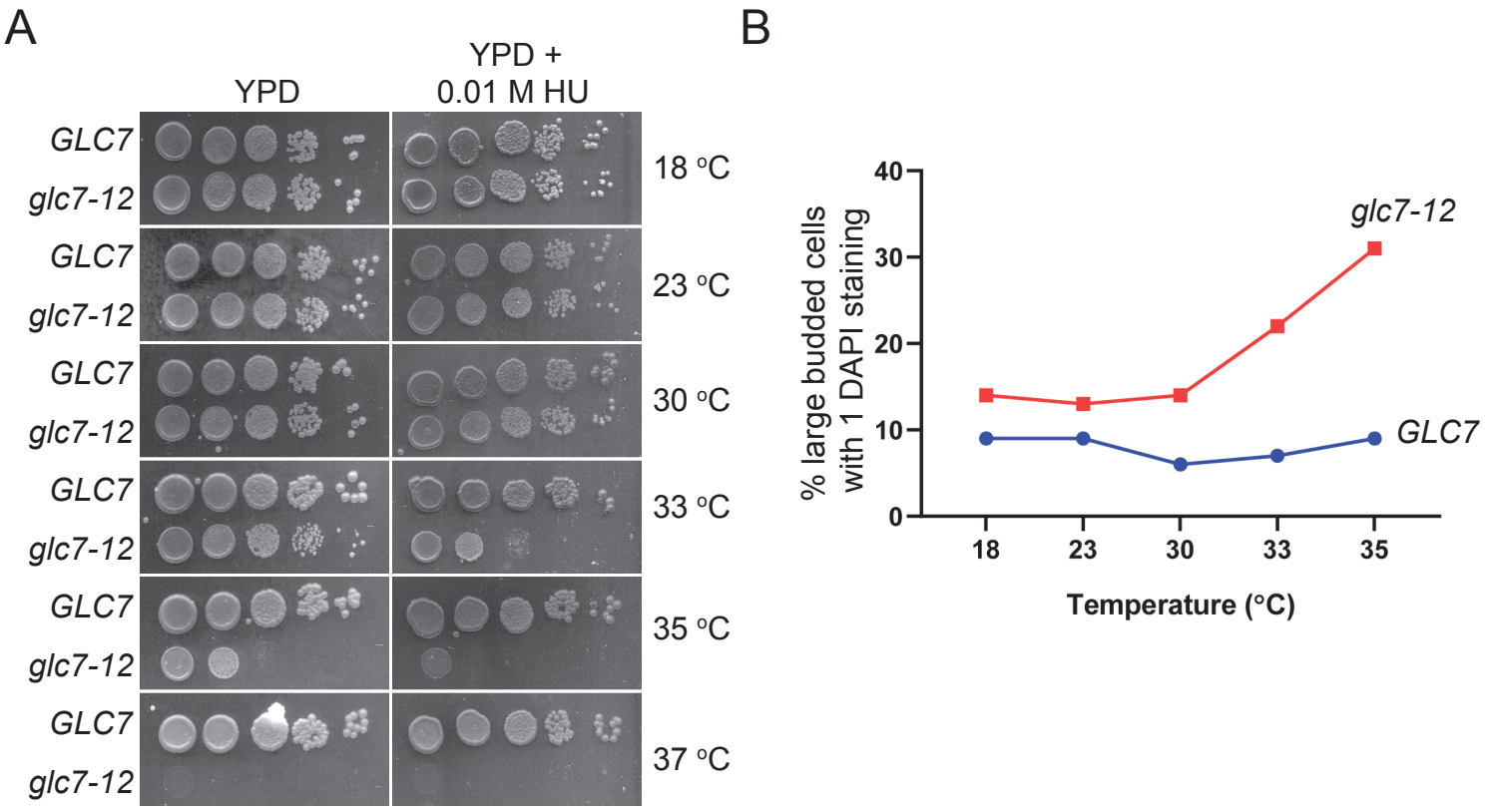

Figure 5 - Figure Supplement 1

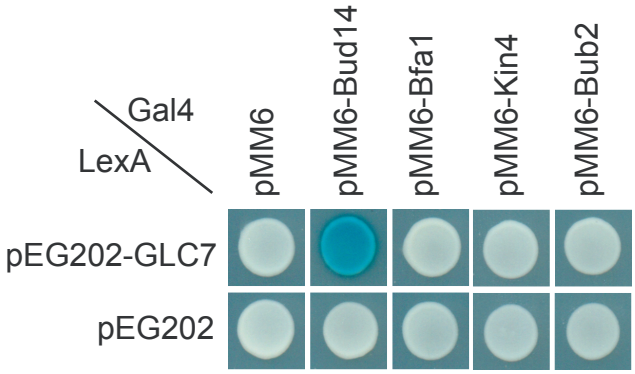

Figure 6 - Figure Supplement 1

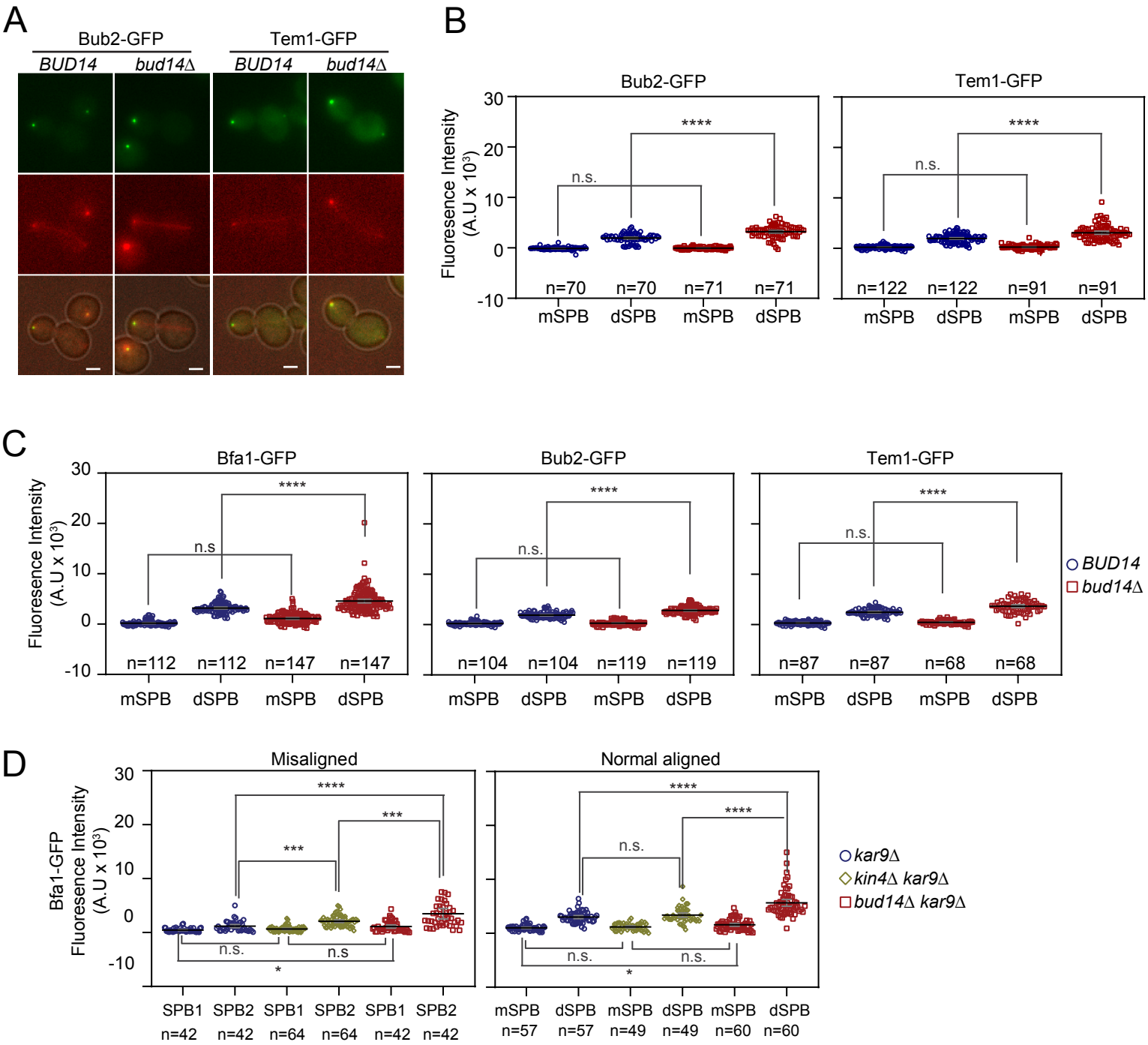

Figure 6 - Figure Supplement 2

A

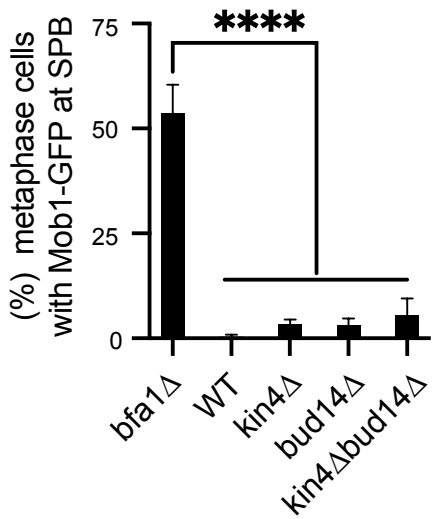

B

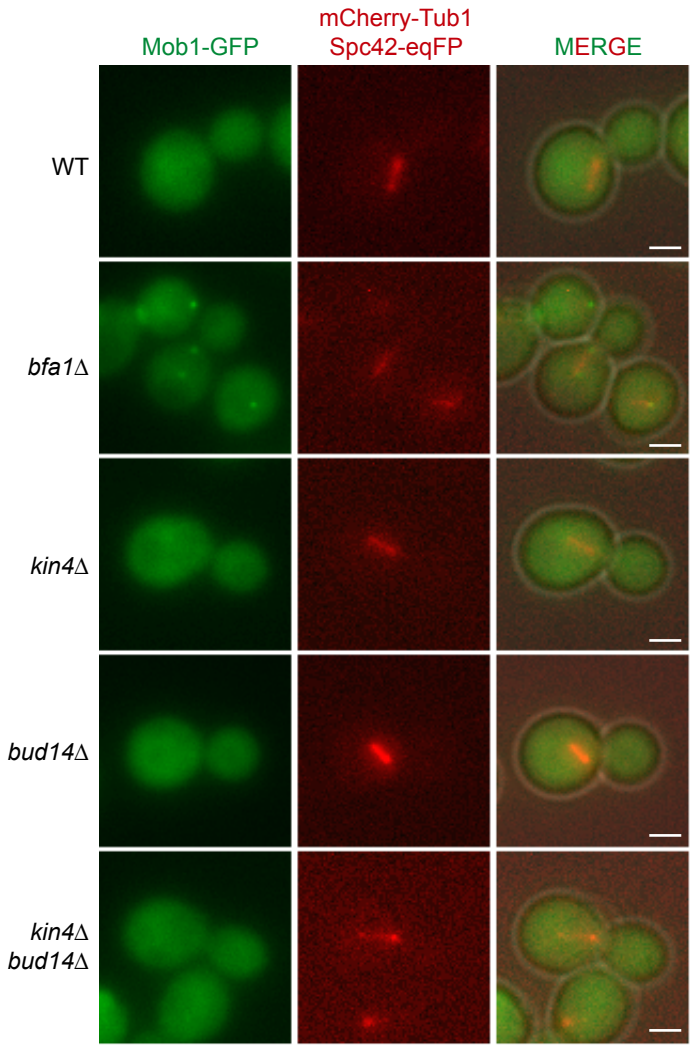

C

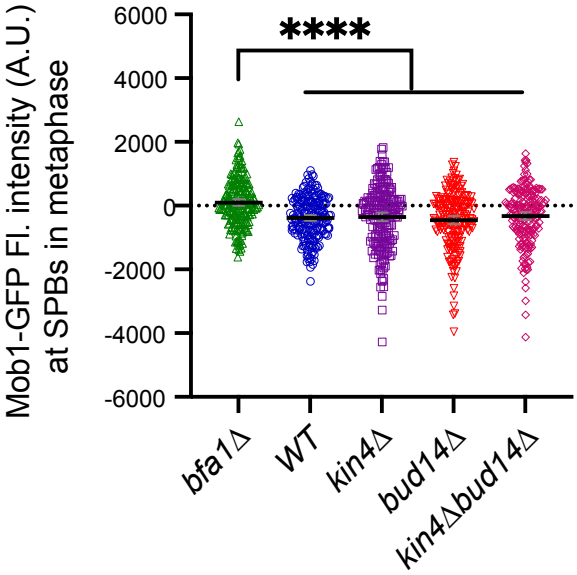

D

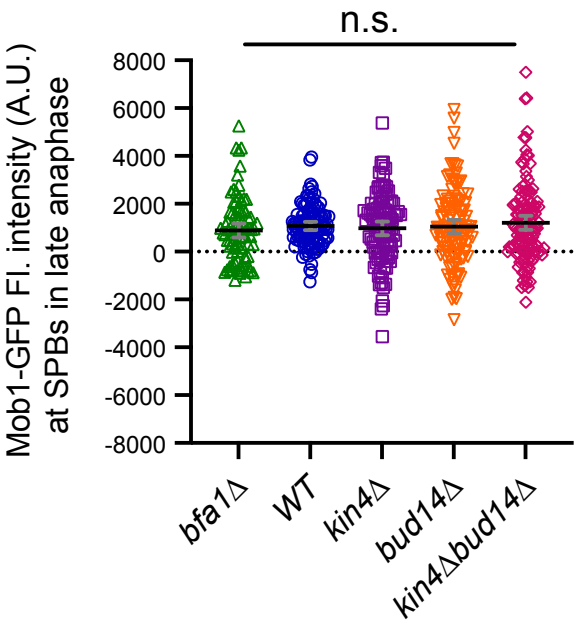

E

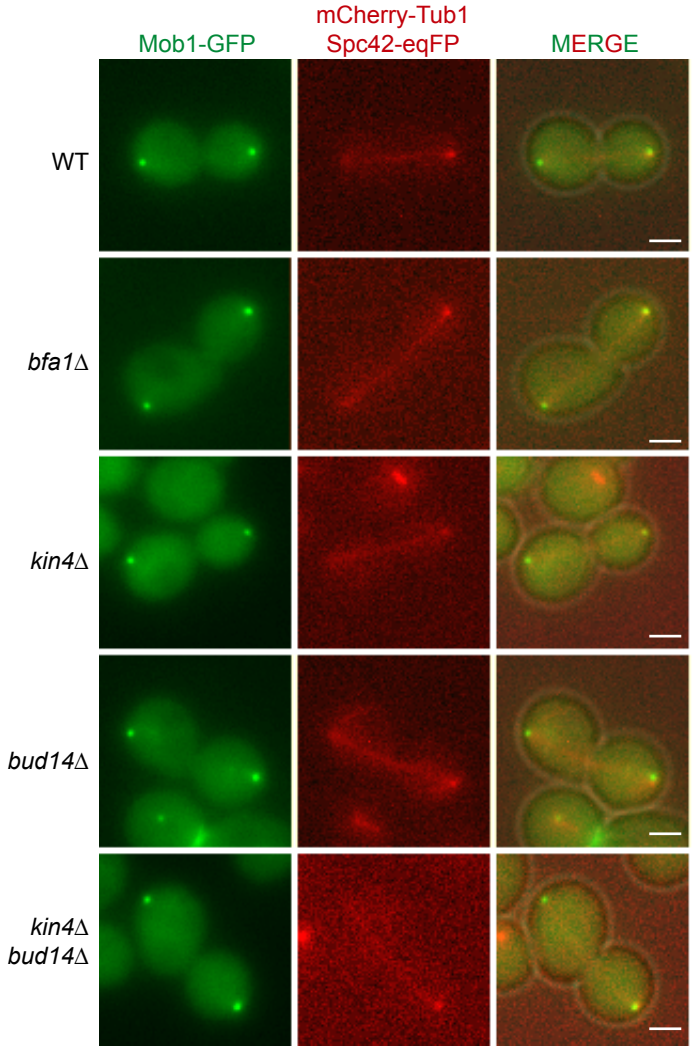

Figure 6 - Figure Supplement 3

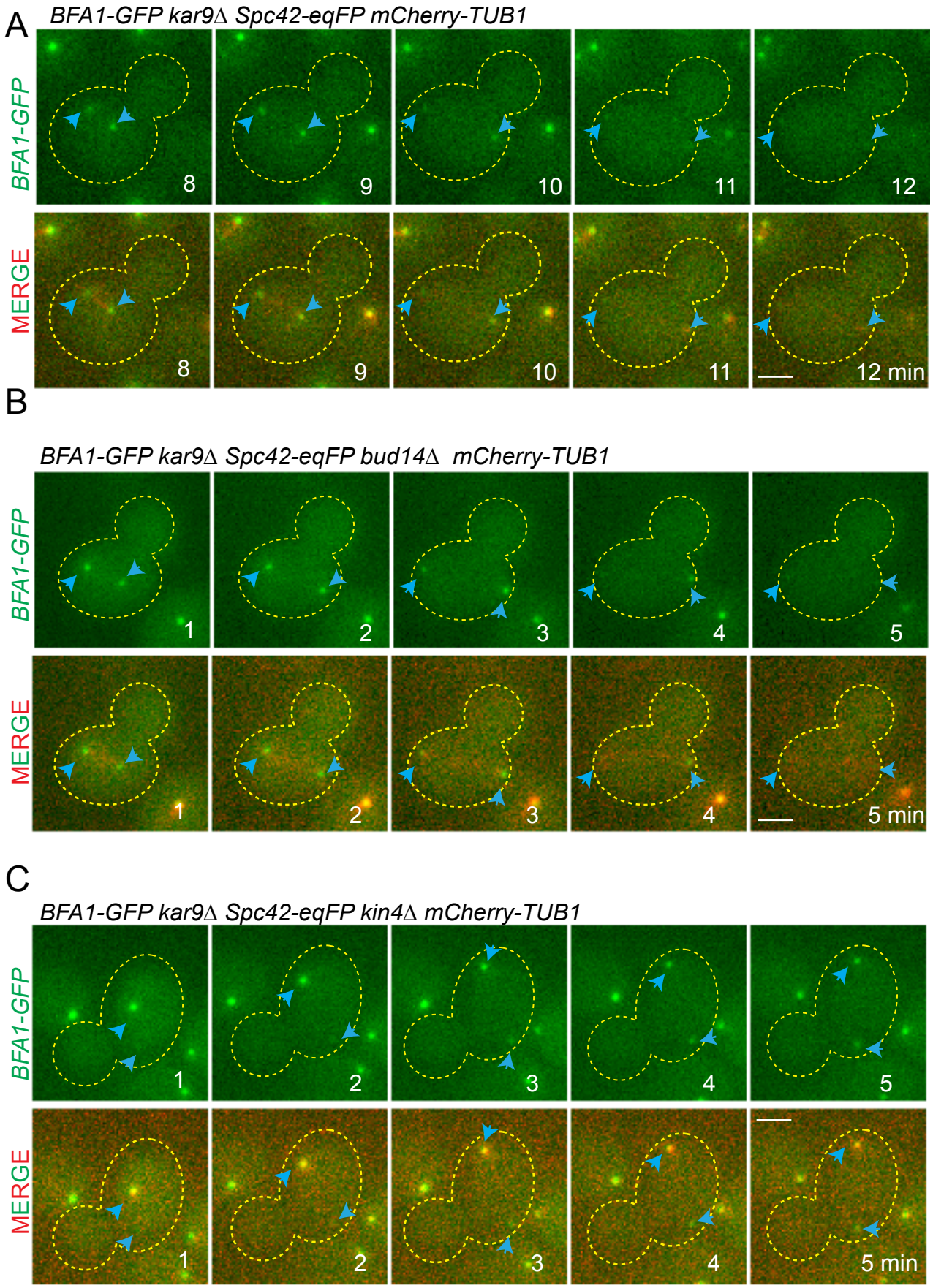

Figure 7 - Figure Supplement 1

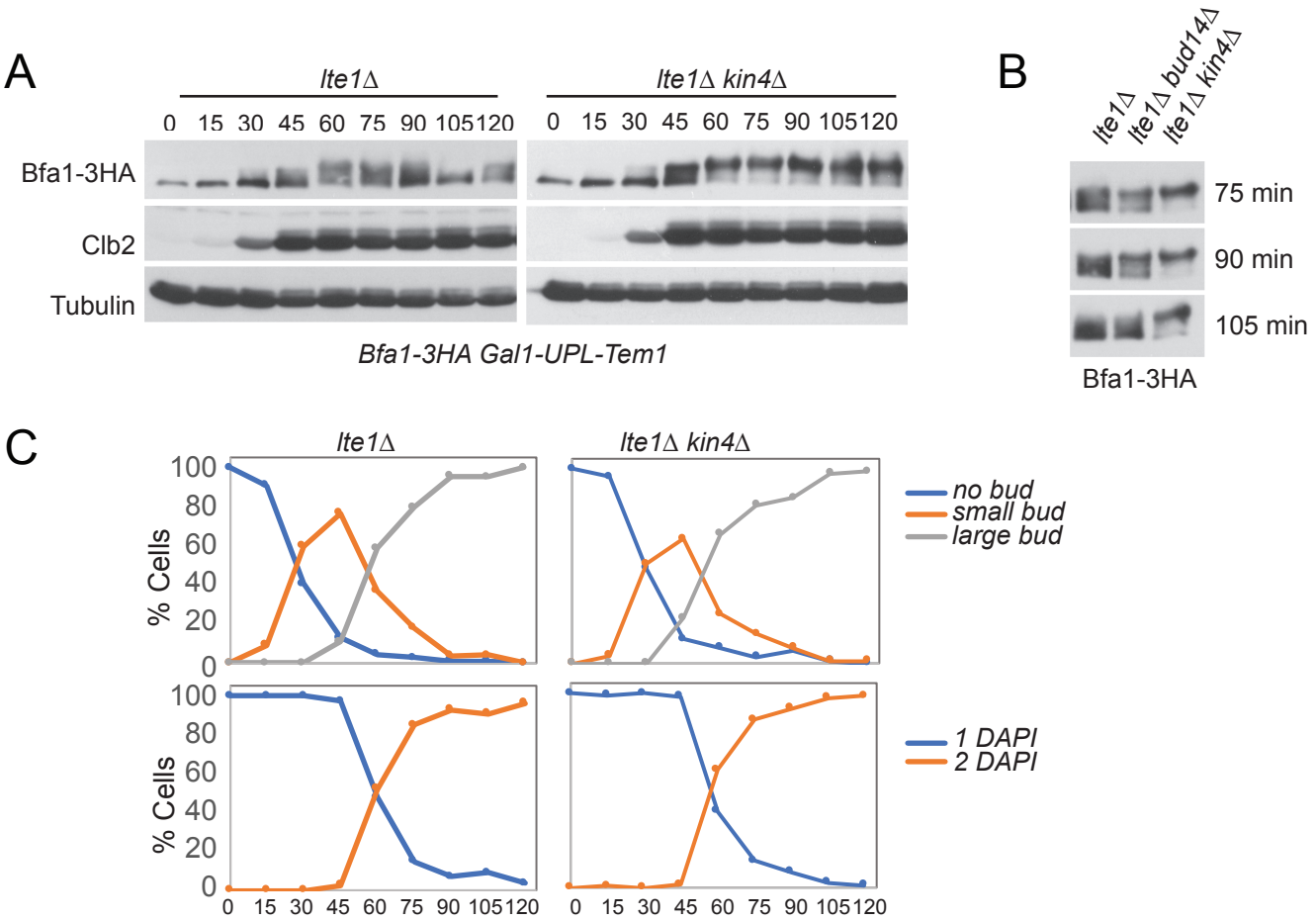

Figure 7 - Figure Supplement 2

A

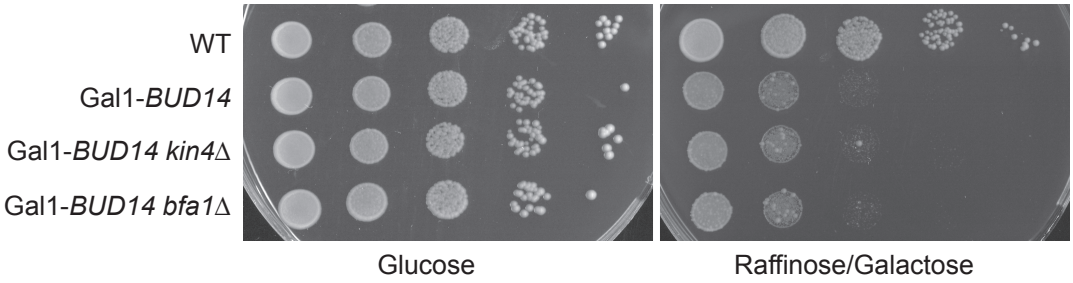
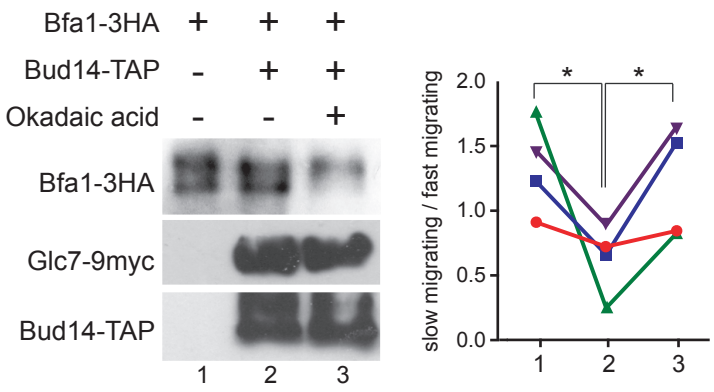
B